gross primary production

Modelling spatial and temporal dynamics of ~~GPP~~ in the Sahel from earth observation based photosynthetic capacity and quantum efficiency

Torbern Tagesson[1], Jonas Ardö[2], Bernard Cappelaere[3], Laurent Kergoat[4], Abdulhakim Abdi[2], Stéphanie Horion[1], Rasmus Fensholt[1]

[1]Department of Geosciences and Natural Resource Management, University of Copenhagen, Øster Voldgade 10, DK-1350 Copenhagen, Denmark; E-Mails: torbern.tagesson@ign.ku.dk, stephanie.horion@ign.ku.dk, rf@ign.ku.dk

[2]Department of Physical Geography and Ecosystem Science, Lund University, Sölvegatan 12, SE- 223 62 Lund, Sweden, E-Mails: jonas.ardo@nateko.lu.se, hakim.abdi@gmail.com

[3]HydroSciences Montpellier, IRD, CNRS, Univ. Montpellier, Montpellier, France, E-Mail: bernard.cappelaere@um2.fr

[4]Geoscience Environnement Toulouse, (CNRS/UPS/IRD), 14 av E Belin, 31400 Toulouse, France, E-Mail: laurent.kergoat@get.obs-mip.fr

Correspondence to: Torbern Tagesson (torbern.tagesson@ign.ku.dk)

Abstract. It has been shown that vegetation growth in semi-arid regions is important to the global terrestrial CO_2 sink, which indicates the strong need for improved understanding and spatially explicit estimates of CO_2 uptake (gross primary production (GPP)) in semi-arid ecosystems. This study has three aims: 1) to evaluate the MOD17A2H GPP (collection 6) product against eddy covariance (EC) based GPP for six sites across the Sahel; 2) to characterize relationships between spatial and temporal variability in EC based photosynthetic capacity (F_{opt}) and quantum efficiency (α) and earth observation (EO) based vegetation indices (normalized difference vegetation index (NDVI); renormalized difference vegetation index (RDVI); enhanced vegetation index (EVI); and shortwave infrared water stress index (SIWSI)); and 3) to study the applicability of EO upscaled F_{opt} and α for GPP modelling purposes. MOD17A2H GPP (collection 6) drastically underestimated GPP, most likely because maximum light use efficiency is set too low for semi-arid ecosystems in the MODIS algorithm. Intra-annual dynamics in F_{opt} were closely related to SIWSI being sensitive to equivalent water thickness, whereas α was closely related to RDVI being affected by chlorophyll abundance. Spatial and inter-annual dynamics in F_{opt} and α were closely coupled to NDVI and RDVI, respectively. Modelled GPP based on F_{opt} and α upscaled using EO based indices reproduced in situ GPP well for all except a cropped site that was strongly impacted by anthropogenic land use. Upscaled GPP for the Sahel 2001-2014 was 736±39 g C m^{-2} y^{-1}. This study indicates the strong applicability of EO as a tool for spatially explicit estimates of GPP, F_{opt} and α; incorporating EO based F_{opt} and α in dynamic global vegetation models could improve global estimates of vegetation production, ecosystem processes and biogeochemical and hydrological cycles.

* do you estimate processes & cycles?

↑ global estimates of ecological processes...?

Keywords: Remote sensing, Gross Primary Productivity, MOD17A2H, light use efficiency, photosynthetic capacity, quantum efficiency

1 Introduction

Vegetation growth in semi-arid regions is an important sink for fossil fuel emissions. Mean carbon dioxide (CO_2) uptake by terrestrial ecosystems is dominated by highly productive lands, mainly tropical forests, whereas semi-arid regions are the main biome driving its inter-annual variability (Ahlström et al., 2015; Poulter et al., 2014). Semi-arid regions even contribute to 60% of the long-term trend in the global terrestrial C sink (Ahlström et al., 2015). It is thus important to understand long-term variability of vegetation growth in semi-arid areas and the response of vegetation to environmental conditions to better quantify and forecast effects of climate change.

The Sahel is a semi-arid transition zone between the dry Sahara desert in the North and the humid Sudanian savanna in the South. The region has experienced numerous severe droughts over the last decades, which resulted in region-wide famines in 1972-1973 and 1984–1985 and localized food shortages across the region in 1990, 2002, 2004, 2011 and 2012 (Abdi et al., 2014; United Nations, 2013). Vegetation production is thereby an important ecosystem service for livelihoods in the Sahel, but it is under threat. The region is experiencing strong population growth, increasing the demand on ecosystem services due to cropland expansion, increased pasture stocking rates and fuelwood extraction (Abdi et al., 2014).

At the same time as we have reports of declining vegetation production, we have contradicting reports of the greening of the Sahel based on earth observation (EO) data (Dardel et al., 2014; Fensholt et al., 2013). The greening of the Sahel has mainly been attributed to alleviated drought stress conditions due to increased precipitation since the mid-1990s (Hickler et al., 2005). Climate is thus another important factor regulating vegetation production. Semi-arid regions, such as the Sahel, are particularly vulnerable to climate fluctuations due to their dependency on moisture.

Estimation of gross primary production (GPP), i.e. uptake of atmospheric CO_2 by vegetation, is still a major challenge for the remote sensing of ecosystem services. Gross primary production is a main driver of ecosystem services such as climate regulation, carbon (C) sequestration, C storage, food production and livestock grassland production. Within EO, spatial quantification of GPP generally involves light use efficiency (LUE), defined as the conversion efficiency of absorbed solar light into CO_2 uptake (Monteith, 1972, 1977). It has been shown that LUE varies in space and time due to factors such as plant functional type, drought and temperature, nutrient levels and physiological limitations of photosynthesis (Garbulsky et al., 2010; Paruelo et al., 2004; Kergoat et al., 2008). The LUE concept has been applied through various methods, either by using a biome-specific LUE constant (Ruimy et al., 1994) or by modifying a maximum LUE using meteorological variables (Running et al., 2004).

An example of a LUE based model is the standard GPP product from the Moderate Resolution Imaging Spectroradiometer (MODIS) sensor (MOD17A2). Within the model, absorbed photosynthetically active radiation (PAR) is estimated as a product of the fraction of PAR absorbed by green vegetation (FPAR from MOD15A2) multiplied with daily PAR from the meteorological data of the Global Modeling and Assimilation Office (GMAO). A set of maximum LUE parameters specified for each biome are extracted from a Biome Properties Look-Up Table (BPLUT). Then maximum LUE is modified depending on air temperature (T_{air}) and vapour pressure deficit (VPD) (Running et al., 2004). Sjöström et al. (2013) evaluated the MOD17A2 product (collection 5.1) for Africa and showed

75 that it underestimated GPP for semi-arid savannas in the Sahel. Explanations for this underestimation were that the
76 assigned maximum LUE from BPLUT was set too low and that there were uncertainties in the FPAR product
77 (MOD15A2). Recently, a new collection of MOD17A2 at a 500 m spatial resolution was released (MOD17A2H;
78 collection 6) with an updated BPLUT, updated GMAO meteorological data, improved quality control and gap-filling of
79 the FPAR data from MOD15A2 (Running and Zhao, 2015).
80 It has been shown that the LUE method does not perform well in arid conditions and at agricultural sites (Turner et
81 al., 2005). Additionally, the linearity assumed by the LUE model is not usually found as the response of GPP to
82 incoming light follows more an asymptotic curve (Cannell and Thornley, 1998). Investigating other methods for
83 remotely determining GPP is thus of great importance, especially for semi-arid environments. Therefore, instead of
84 LUE, we focus on the light response function of GPP at the canopy scale, and spatial and temporal variation of its two
85 main parameters: maximum GPP under light saturation (canopy-scale photosynthetic capacity; F_{opt}) and the initial slope
86 of the light response function (canopy-scale quantum efficiency; α) (Falge et al., 2001; Tagesson et al., 2015a).
87 Photosynthetic capacity is a measure of the maximum rate at which the canopy can fix CO_2 during photosynthesis
88 ($\mu mol\ CO_2\ m^{-2}\ s^{-1}$), whereas α is the amount of CO_2 fixed per incoming PAR ($\mu mol\ CO_2\ \mu mol\ PAR^{-1}$). To clarify the
89 difference in LUE and α in this study, LUE ($\mu mol\ CO_2\ \mu mol\ APAR^{-1}$) is the slope of a linear fit between CO_2 uptake
90 and absorbed PAR, whereas α ($\mu mol\ CO_2\ \mu mol\ PAR^{-1}$) is the initial slope of an asymptotic curve against incoming
91 PAR.
92 It has been proven that F_{opt} and α are closely related to chlorophyll abundance due to their coupling with the electron
93 transport rate (Ide et al., 2010). Additionally, in semi-arid ecosystems, water availability is generally considered to be
94 the main limiting factor affecting intra-annual dynamics of vegetation growth (Fensholt et al., 2013; Hickler et al.,
95 2005; Tagesson et al., 2015b). Several remote sensing studies have established relationships between remotely sensed
96 vegetation indices and ecosystem properties such as chlorophyll abundance and equivalent water thickness (Yoder and
97 Pettigrew-Crosby, 1995; Fensholt and Sandholt, 2003). In this study, we will analyse whether EO vegetation indices
98 can be used to upscale F_{opt} and α and investigate whether this could offer a promising way to map GPP in semi-arid
99 areas. This potential will be analysed by the use of detailed ground observations from six eddy covariance (EC) flux
100 tower sites across the Sahel.
101 The three aims of this study are:
102 1) To investigate whether the recently released MOD17A2H GPP (collection 6) product is better at capturing
103 GPP for the Sahel than collection 5.1. We hypothesize that the MOD17A2H GPP (collection 6) product will
104 estimate GPP well for the six Sahelian EC sites because of major changes made in comparison to collection
105 5.1 (Running and Zhao, 2015).
106 2) To characterize the relationships between spatial and temporal variability in F_{opt} and α and remotely sensed
107 vegetation indices. We hypothesise that EO vegetation indices that are closely related to chlorophyll
108 abundance will be most strongly coupled with spatial and inter-annual dynamics in F_{opt} and α, whereas
109 vegetation indices closely related to equivalent water thickness will be most strongly coupled with intra-annual
110 dynamics in F_{opt} and α across the Sahel.
111 3) To evaluate the applicability of a GPP model based on the light response function using EO vegetation indices
112 and incoming PAR as input data.
113

2 Materials and Methods

2.1 Site description

The Sahel stretches from the Atlantic Ocean in the west to the Red Sea in the east. The northern border towards the Sahara and the southern border towards the humid Sudanian Savanna are defined by the 150 and 700 mm isohyets, respectively (Fig. 1) (Prince et al., 1995). Tree and shrub canopy cover is now generally low (< 5%) and dominated by species of *Balanites*, *Acacia, Boscia* and *Combretaceae* (Rietkerk et al., 1996). Annual grasses such as *Schoenefeldia gracilis*, *Dactyloctenium aegypticum*, *Aristida mutabilis* and *Cenchrus biflorus* dominate the herbaceous layer, but perennial grasses such as *Andropogon gayanus*, *Cymbopogon schoenanthus* can also be found (Rietkerk et al., 1996; de Ridder et al., 1982). From the FLUXNET database (Baldocchi et al., 2001) we selected the six available measurement sites with EC based CO_2 flux data from the Sahel (Table 1; Fig. 1). The sites represent a variety of ecosystems present in the region, from dry fallow bush savanna to seasonally inundated acacia forest. For a full description of the measurement sites, we refer to Tagesson et al. (2016a) and references in Table 1.

<Table 1>

<Figure 1>

2.2 Data collection

2.2.1 Eddy covariance and hydrometeorological in situ data

Eddy covariance and hydrometeorological data originating from the years between 2005 and 2013 were collected from the principal investigators of the measurement sites (Tagesson et al., 2016a). The EC sensor setup consisted of open-path CO_2/H_2O infrared gas analysers and 3-axis sonic anemometers. Data were collected at 20 Hz rate and statistics were calculated for 30-minute periods. For a full description of the sensor setup and post processing of EC data, see the references in Table 1. Final fluxes were filtered according to quality flags provided by FLUXNET and outliers were filtered according to Papale et al. (2006). We extracted the original net ecosystem exchange (NEE) data without any gap-filling or partitioning of NEE to GPP and ecosystem respiration. The collected hydrometeorological data were: air temperature (T_{air}; °C), rainfall (P; mm), relative air humidity (Rh; %), soil moisture at 0.1 m depth (SWC; % volumetric water content), incoming global radiation (R_g; W m^{-2}), incoming photosynthetically active radiation (PAR; µmol m^{-2} s^{-1}), VPD (hPa), peak dry weight biomass (g dry weight m^{-2}), C3/C4 species ratio and soil conditions (nitrogen and C concentration; %). For a full description of the collected data and sensor setup, see Tagesson et al. (2016a).

2.2.2 Earth Observation data and gridded ancillary data

Composite products from MODIS/Terra covering the Sahel were acquired at Reverb ECHO (NASA, 2016). Collected products were GPP (MOD17A2H; collection 6), nadir bidirectional reflectance distribution function adjusted reflectance (NBAR) (8-day composites; MCD43A4; collection 5.1) at 500×500 m^2 spatial resolution, the normalized difference vegetation index (NDVI) and the enhanced vegetation index (EVI) (16-day composites; MOD13Q1; collection 6) at 250×250 m^2 spatial resolution. The NBAR product was preferred over the reflectance product (MOD09A1) in order to avoid variability caused by varying sun and sensor viewing geometry (Huber et al., 2014; Tagesson et al., 2015c). We extracted the median of 3x3 pixels centred at the location of each EC tower. Time series of EO products were filtered according to MODIS quality control data; MOD17A2H is a gap-filled and filtered product,

QC data from MCD43A2 were used for filtering of MCD43A4; and bit 2-5 (highest –decreasing quality) was used for MOD13Q1. Finally, data were gap-filled to daily values using linear interpolation.

We downloaded ERA Interim reanalysis PAR at the ground surface (W m^{-2}) with a spatial resolution of 0.25°×0.25° accumulated for each 3-hour period from 2000-2015 from the European Centre for Medium-Range Weather Forecasts (ECMWF) (Dee et al., 2011; ECMWF, 2016a).

2.3 Data handling

2.3.1 Intra-annual dynamics in photosynthetic capacity and quantum efficiency

To estimate daily values of EC based F_{opt} and α, the asymptotic Mitscherlich light-response function was fitted between daytime NEE and incoming PAR using a 7-day moving window with a 1-day time step:

$$NEE = -(F_{opt}) \times (1 - e^{\left(\frac{-\alpha \times PAR}{F_{opt}}\right)}) + R_d \quad (1)$$

where F_{opt} is CO_2 uptake at light saturation (photosynthetic capacity; μmol CO_2 m^{-2} s^{-1}), R_d is dark respiration (μmol CO_2 m^{-2} s^{-1}) and α is the initial slope of the light response curve (quantum efficiency; μmol CO_2 μmol PAR^{-1}) (Falge et al., 2001). By subtracting R_d from Eq. 1, the function was forced through zero and GPP was thereby estimated. To ensure a high quality of fitted parameters, parameters were excluded from the analysis when fitting was insignificant (p-value>0.05) and when they were out of range (F_{opt} and α >peak value of the rainy season times 1.2). Additionally, outliers were filtered following the method by Papale et al. (2006) using a 30-day moving window with a 1-day time step.

2.3.2 Vegetation indices

The maximum absorption in red wavelengths generally occurs at 682 nm as this is the peak absorption for chlorophyll a and b (Thenkabail et al., 2000), which makes vegetation indices that include the red band sensitive to chlorophyll abundance. By far the most common vegetation index is NDVI (Rouse et al., 1974):

$$NDVI = \frac{(\rho_{NIR} - \rho_{red})}{(\rho_{NIR} + \rho_{red})} \quad (2)$$

where ρ_{NIR} is the reflectance factor in the near infrared (NIR) band (band 2) and ρ_{red} is the reflectance factor in the red band (band 1). Near infrared radiance is reflected by leaf cells since absorption of these wavelengths would result in overheating of the plant, whereas red radiance is absorbed by chlorophyll and its accessory pigments (Gates et al., 1965). Normalization is done to reduce effects of atmospheric errors, solar zenith angles and sensor viewing geometry, as well as to increase the vegetation signal (Qi et al., 1994; Inoue et al., 2008).

A well-known deficiency of NDVI is problems of index saturation at high biomass because absorption of red light at ~670 nm peaks at higher biomass loads, whereas NIR reflectance continues to increase due to multiple scattering effects (Mutanga and Skidmore, 2004; Jin and Eklundh, 2014). By reducing atmospheric and soil background influences, EVI is designed to increase the signal from the vegetation and maintain sensitivity in high biomass regions (Huete et al., 2002).

$$EVI = G\frac{(\rho_{NIR} - \rho_{red})}{(\rho_{NIR} + C_1\rho_{red} - C_2\rho_{blue} + L)} \quad (3)$$

where ρ_{blue} is the reflectance factor in the blue band (band 3). The coefficients C_1=6 and C_2=7.5 correct for atmospheric influences, while L=1 adjusts for the canopy background. The factor G=2.5 is a gain factor.

Another attempt to overcome problems of NDVI saturation was proposed by Roujean and Breon (1995), who suggested the renormalized difference vegetation index (RDVI), which combines advantages of DVI (NIR-red) and NDVI for low and high vegetation cover, respectively:

$$RDVI = \frac{(\rho_{NIR} - \rho_{red})}{\sqrt{(\rho_{NIR} + \rho_{red})}} \quad (4)$$

As a non-linear index, RDVI is not only less sensitive to variations in geometrical and optical properties of unknown foliage but also less affected by solar and viewing geometry (Broge and Leblanc, 2001). The vegetation index RDVI was calculated based on NBAR bands 1 and 2.

The NIR and SWIR bands are affected by the same ground properties, except that SWIR bands are also strongly sensitive to equivalent water thickness. Fensholt and Sandholt (2003) proposed a vegetation index, the shortwave infrared water stress index (SIWSI), using NIR and SWIR bands to estimate drought stress for vegetation in semi-arid environments:

$$SIWSI_{12} = \frac{(\rho_{NIR} - \rho_{SWIR12})}{(\rho_{NIR} + \rho_{SWIR12})} \quad (5)$$

$$SIWSI_{16} = \frac{(\rho_{NIR} - \rho_{SWIR16})}{(\rho_{NIR} + \rho_{SWIR16})} \quad (6)$$

where ρ_{swir12} is NBAR band 5 (1230-1250 nm) and ρ_{swir16} is NBAR band 6 (1628-1652 nm). As the vegetation water content increases, reflectance in SWIR decreases, indicating that low and high SIWSI values point to sufficient water conditions and drought stress, respectively.

2.3.3 Incoming PAR across the Sahel

A modified version of the ERA Interim reanalysis PAR was used in the current study as there was an error in the code producing these PAR estimates; the estimates were generally too low (ECMWF, 2016b). Accordingly, incoming PAR at the ground surface from ERA Interim was systematically underestimated even though it followed the pattern of PAR measured at the six Sahelian EC sites (Fig. S1 in supplementary material). In order to correct for this error, we fitted and applied an ordinary least squares linear regression between in situ PAR and ERA Interim PAR (Fig. S1). The PAR produced from this relationship is at the same level as in situ PAR and should be at a correct level even though the original ERA Interim PAR is actually produced from the red and near infrared part of the spectrum.

2.4 Data analysis

2.4.1 Coupling temporal and spatial dynamics in photosynthetic capacity and quantum efficiency with explanatory variables

The coupling between intra-annual dynamics in F_{opt} and α and the vegetation indices for the different measurement sites were studied using Pearson correlation analysis. As part of the correlation analysis, we used a bootstrap simulation methodology with 200 iterations from which the mean and the standard deviation of the correlation coefficients were calculated (Richter et al., 2012). Relationships between intra-annual dynamics in F_{opt} and α and the vegetation indices

for all sites combined were also analysed. In the analysis for all sites, data were normalized to avoid influence of spatial and inter-annual variability. Time series of ratios of F_{opt} and α (F_{opt_frac} and α_{frac}) against the annual peak values (F_{opt_peak} and α_{peak}; see below for calculation of annual peak values) were estimated for all sites:

$$F_{opt\_frac} = \frac{F_{opt}}{F_{opt\_peak}} \quad (7)$$

$$\alpha_{frac} = \frac{\alpha}{\alpha_{peak}} \quad (8)$$

The same standardization procedure was used for all vegetation indices (VI_{frac}):

$$VI_{frac} = \frac{VI}{VI_{peak}} \quad (9)$$

where VI_{peak} is the annual peak values of the vegetation indices (14-day running mean with highest annual value). The α_{frac} and F_{opt_frac} were correlated with the different VI_{frac} to investigate the coupling between intra-annual dynamics in F_{opt} and α and the vegetation indices for all sites.

Regression trees were used to fill gaps in the daily estimates of F_{opt} and α. One hundred tree sizes were chosen based on 100 cross-validation runs, and these trees were then used to estimate F_{opt} and α following the method in De'ath and Fabricius (2000). We used SWC, VPD, T_{air}, PAR and the vegetation index with the strongest correlation with intra-annual dynamics as explanatory variables in the analysis. In the analysis for all sites, the same standardization procedure as done for F_{opt}, α, and the vegetation indices was done for the hydrometeorological variables. The 100 F_{opt} and α output subsets from the regression trees were averaged and used for filling gaps in the times series of F_{opt} and α. From these time series, we estimated annual peak values of F_{opt} and α (F_{opt_peak} and α_{peak}) as the 14-day running mean with the highest annual value. To investigate spatial and inter-annual variability in F_{opt} and α across the measurement sites of the Sahel, F_{opt_peak} and α_{peak} were correlated with the annual sum of P; yearly means of T_{air}, SWC, RH, VPD and R_g; annual peak values of biomass; soil nitrogen and C concentrations; the C3/C4 ratio; and VI_{peak}.

2.4.2 Parameterization and evaluation of the GPP model and evaluation of the MODIS GPP

On the basis of Eq. 1 and the outcome of the statistical analysis previously described under subsection 2.4.1 (for results, see subsect. 3.2), a model for estimating GPP across the Sahel was created:

$$GPP = -F_{opt} \times \left(1 - e^{\left(\frac{-\alpha \times PAR}{F_{opt}}\right)}\right) \quad (10)$$

Firstly, F_{opt_peak} and α_{peak} were estimated spatially and inter-annually using linear regression functions fitted against the vegetation indices with strongest relationships to spatial and inter-annual variability in F_{opt_peak} and α_{peak} for all sites. Secondly, exponential regression functions were established for F_{opt_frac} and α_{frac} with the vegetation index with the strongest relationships to intra-annual variability of F_{opt_frac} and α_{frac} for all sites. By combining these relationships, F_{opt} and α can be calculated for any day of year and for any point in space across the Sahel:

$$F_{opt} = F_{opt\_peak} \times F_{opt\_frac} = \left(k_{Fopt} \times NDVI_{peak} + m_{Fopt}\right)\left(n_{Fopt} \times e^{\left(l_{Fopt} \times RDVI_{frac}\right)}\right) \quad (11)$$

$$\alpha = \alpha_{peak} \times \alpha_{frac} = \left(k_{\alpha} \times RDVI_{peak} + m_{\alpha}\right)\left(n_{\alpha} \times e^{\left(l_{\alpha} \times RDVI_{frac}\right)}\right) \quad (12)$$

where k_{Fopt} and k_{α} are slopes and m_{Fopt} and m_{α} are intercepts of the linear regressions giving F_{opt_peak} and α_{peak}, respectively; l_{Fopt} and l_{α} are coefficients and n_{Fopt} and n_{α} are intercepts of the exponential regressions giving F_{opt_frac} and α_{frac}, respectively. Equations 11 and 12 were inserted into Eq. 10, and GPP was thereby estimated as:

$$GPP = -\left(F_{opt\_peak} \times F_{opt\_frac}\right) \times \left(1 - e^{\left(\frac{-\left(\alpha_{peak} \times \alpha_{frac}\right) \times PAR}{F_{opt\_peak} \times F_{opt\_frac}}\right)}\right) = -\left(\left(k_{Fopt} \times NDVI_{peak} + m_{Fopt}\right)\left(n_{Fopt} \times e^{\left(l_{Fopt} \times RDVI_{frac}\right)}\right)\right) \times \left(1 - e^{\left(\frac{-\left(k_{\alpha} \times RDVI_{peak} + m_{\alpha}\right)\left(n_{\alpha} \times e^{\left(l_{\alpha} \times RDVI_{frac}\right)}\right) \times PAR}{\left(k_{Fopt} \times NDVI_{peak} + m_{Fopt}\right)\left(l_{Fopt} \times RDVI_{frac} + n_{Fopt}\right)}\right)}\right) \quad (13)$$

The bootstrap simulation methodology was used when fitting the least squares regression functions for parameterization of the GPP model (Richter et al., 2012). For each of the iterations, some of the EC sites were included and some were omitted. The bootstrap simulations generated 200 sets of k_{Fopt}, k_{α}, m_{Fopt}, m_{α}, l_{Fopt}, l_{α}, n_{Fopt}, n_{α} and coefficient of determination (R^2). Possible errors (e.g. random sampling errors, aerosols, electrical sensor noise, filtering and gap-filling errors, clouds and satellite sensor degradation) can be present in both the predictor and the response variables. Hence, we selected reduced major axis regressions to account for errors in both predictor and response variables when fitting the regression functions. The regression models were validated against the omitted sites within the bootstrap simulation methodology by calculating the root mean square error (RMSE), and by fitting an ordinary least squares linear regression between modelled and independent variables.

Similarly, the MODIS GPP product (MOD17A2H; collection 6) was evaluated against independent GPP from the EC sites by calculating the RMSE and by fitting an ordinary least squares linear regression.

3 Results

3.1 Evaluation of the MODIS GPP product

There was a strong linear relationship between the MODIS GPP product (MOD17A2H; collection 6) and independent GPP (slope=0.17; intercept=0.11 g C m^{-2} d^{-1}; R^2=0.69; n=598). However, MOD17A2H strongly underestimated independent GPP (Fig. 2), resulting in a high RMSE (2.69 g C m^{-2} d^{-1}). It can be seen that some points for the Kelma site were quite low for MOD17A2H, whereas they were relatively high for the independent GPP (Fig. 2). Kelma is an inundated Acacia forest located in a clay soil depression. These differentiated values were found in the beginning of the dry season, when the depression was still inundated, whereas the larger area was turning dry.

<Figure 2>

3.2 Intra-annual dynamics in photosynthetic capacity and quantum efficiency

Intra-annual dynamics in F_{opt} and α differed in amplitude, but were otherwise similar across the measurement sites in the Sahel (Fig. 3). There was no green ground vegetation during the dry season, and the low photosynthetic activity was due to few evergreen trees. This resulted in low values for both F_{opt} and α during the dry season. The vegetation responded strongly to rainfall, and both F_{opt} and α increased during the early phase of the rainy season. Generally, F_{opt} peaked slightly earlier than α (average± 1 standard deviation: 7±10 days) (Fig. 3).

<Figure 3>

All vegetation indices described intra-annual dynamics in F_{opt} reasonably well at all sites (Table 2). The vegetation index $SIWSI_{12}$ had the highest correlation for all sites except Wankama Millet, where it was RDVI. When all sites were combined, all indices described well seasonality in F_{opt}, but RDVI had the strongest correlation (Table 2).

Intra-annual dynamics in α were also closely coupled to intra-annual dynamics in the vegetation indices for all sites (Table 2). For α, RDVI was the strongest index describing intra-annual dynamics, except for Wankama Fallow, where it was EVI. When all sites were combined, all indices described well intra-annual dynamics in α, but RDVI was still the index with strongest relationship (Table 2).

<Table 2>

The regression trees used for gap-filling explained the intra-annual dynamics in F_{opt} and α well for all sites (Table 3; Fig. S2 in Supplementary material). The regression trees explained intra-annual dynamics in F_{opt} better than in α, and multi-year sites were better predicted than single year sites (Fig. S2). The main explanatory variables coupled to intra-annual dynamics in F_{opt} for all sites across the Sahel were in the order of RDVI, SWC, VPD, T_{air}, and PAR; and for α, they were RDVI, SWC, VPD and T_{air} (Table 3). The strong relationship to SWC and VPD indicates drought stress during periods of low rainfall. For all sites across the Sahel, incorporating hydrometeorological variables increased the ability to determine intra-annual dynamics in F_{opt} and α compared to the ordinary least squares linear regressions against vegetation indices (Table 2, data given as *r;* Table 3; Fig. 3 and Fig. S2). For all sites, incorporation of these variables increased R^2 from 0.81 to 0.87 and from 0.74 to 0.84 for F_{opt} and α, respectively.

<Table 3>

3.3 Spatial and inter-annual dynamics in photosynthetic capacity and quantum efficiency

Large spatial and inter-annual variability in F_{opt_peak} and α_{peak} were found across the six measurement sites in the Sahel; F_{opt_peak} ranged between 10.1 μmol CO_2 m^{-2} s^{-1} (Wankama Millet 2005) and 50.0 μmol CO_2 m^{-2} s^{-1} (Dahra 2010), and α_{peak} ranged between 0.020 μmol CO_2 μmol PAR^{-1} (Demokeya 2007) and 0.064 μmol CO_2 μmol PAR^{-1} (Dahra 2010) (Table 4). The average 2-week running mean peak values of F_{opt} and α for all sites were 26.4 μmol CO_2 m^{-2} s^{-1} and 0.040 μmol CO_2 μmol PAR^{-1}, respectively. All vegetation indices determined spatial and inter-annual dynamics well in both F_{opt_peak} and α_{peak} (Table 5); F_{opt_peak} was most closely coupled with $NDVI_{peak}$, whereas α_{peak} was coupled more closely with $RDVI_{peak}$ (Fig. 4). F_{opt_peak} also correlated well with peak dry weight biomass, C content in the soil, and RH, whereas α_{peak} ~~was~~ correlated ~~well~~ with peak dry weight biomass and C content in the soil (Table 5).

<Table 4>

<Table 5>

<Figure 4>

3.4 Spatially extrapolated photosynthetic capacity, quantum efficiency and gross primary production across the Sahel and evaluation of the GPP model

The spatially extrapolated F_{opt}, α and GPP averaged over the Sahel for 2001-2014 were 22.5±1.7 μmol CO_2 m^{-2} s^{-1}, 0.030±0.002 μmol CO_2 μmol PAR^{-1} and 736±39 g C m^{-2} y^{-1}, respectively. At a regional scale, it can be seen that F_{opt}, α and GPP decreased substantially with latitude (Fig. 5). The highest values were found in south-eastern Senegal, western Mali, in parts of southern Sudan and on the border between Sudan and South Sudan. Lowest values were found along the northernmost parts of the Sahel on the border to the Sahara in Mauritania, in northern Mali and in northern Niger.

Modelled GPP was similar to independent GPP on average, and there was a strong linear relationship between modelled GPP and independent GPP for all sites (Fig. 6; Table 6). However, when separating the evaluation between measurement sites, it can be seen that the model reproduced some sites better than others (Fig. 7; Table 6). Wankama Millet was generally overestimated, whereas the model worked well on average for Demokeya but underestimated high values (Fig. 7; Table 6). Variability of independent GPP at the other sites was well reproduced by the model (Fig. 7; Table 6). The final parameters of the GPP model (Eq. 13) are shown in Table 7.

<Figure 5>

<Figure 6>

<Figure 7>

< Table 6>

< Table 7>

4 Discussion

Our hypothesis that vegetation indices closely related to equivalent water thickness (SIWSI) would be most strongly coupled with intra-annual dynamics in F_{opt} and α was not rejected for F_{opt}, since this was the case for all sites except for Wankama Millet (Table 2). However, our hypothesis was rejected for α, since it was more closely related to vegetation indices of chlorophyll abundance (RDVI and EVI). In the Sahel, soil moisture conditions in the early rainy season are important for vegetation growth and during this phase vegetation is especially vulnerable to drought conditions (Rockström and de Rouw, 1997; Tagesson et al., 2016a; Mbow et al., 2013). Photosynthetic capacity (F_{opt}) peaked earlier in the rainy season than α did (Fig. 3), thereby explaining the close relationship of F_{opt} to SIWSI. Leaf area index increased over the growing season and leaf area index is closely coupled with vegetation indices related to chlorophyll abundance (Tagesson et al., 2009). The increase in leaf area index increased canopy level quantum efficiency (α), thereby explaining the closer relationship of α to RDVI.

Our hypothesis that vegetation indices closely related to chlorophyll abundance would be most strongly coupled with spatial and inter-annual dynamics in F_{opt} and α was not rejected for either F_{opt} or α; NDVI, EVI and RDVI all correlated with spatial and inter-annual dynamics in F_{opt} and α (Table 5). However, it was surprising that $NDVI_{peak}$ had the strongest correlation with spatial and inter-annual variability for F_{opt} (Table 5). Both EVI and RDVI should be less sensitive to saturation effects than NDVI (Huete et al., 2002; Roujean and Breon, 1995), and based on this it can be assumed that peak values of these indices should have stronger relationships to peak values of F_{opt} and α. However, vegetation indices with a high sensitivity to changes in green biomass at high biomass loads become less sensitive to green biomass changes at low biomass loads (Huete et al., 2002). The peak leaf area index for ecosystems across the Sahel is generally ~2 m^2 m^{-2} or less, whereas the saturation issue of NDVI generally starts at a leaf area index of about 2-5 m^2 m^{-2} (Haboudane et al., 2004).

The F_{opt_peak} estimates from Agoufou, Demokeya and the Wankama sites were similar, whereas Dahra and Kelma values were high in relation to previously reported canopy-scale F_{opt_peak} from the Sahel (~-8 to -23 µmol m^{-2} sec^{-1})(Hanan et al., 1998; Merbold et al., 2009; Moncrieff et al., 1997; Boulain et al., 2009; Levy et al., 1997; Monteny et al., 1997). These previous studies reported much lower F_{opt} at canopy scale than at leaf scale (e.g. Levy et al. (1997): 10 vs. 44 µmol m^{-2} sec^{-1}; Boulain et al. (2009): 8 vs. 50 µmol m^{-2} sec^{-1}). The leaf area index at Dahra and Kelma peaked at 2.1 and 2.7, respectively (Timouk et al., 2009; Tagesson et al., 2015a), and it was substantially higher than at the above-

mentioned sites. A possible explanation for high F_{opt} estimates at Dahra and Kelma could therefore be the higher leaf area index. Tagesson et al. (2016b) performed a quality check of the EC data due to the high net CO_2 exchange measured at the Dahra field site and explained the high values by a combination of moderately dense herbaceous C4 ground vegetation, high soil nutrient availability, and a grazing pressure resulting in compensatory growth and fertilization effects. Another possible explanation could be that the West African Monsoon brings a humid layer of surface air from the Atlantic, possibly increasing vegetation production for the most western part of the Sahel (Tagesson et al., 2016a).

Our model substantially overestimated GPP for Wankama Millet (Fig. 7f). Being a crop field, this site differed from the other sites in its species composition and ecosystem structure, as well as land and vegetation management. Crop fields in southwestern Niger are generally characterized by rather low production, resulting from decreased fertility and soil loss caused by intensive land use (Cappelaere et al., 2009). These specifics of the Wankama Millet site may cause the model, parameterized with observations from the other study sites without this strong anthropogenic influence, to overestimate GPP at this site. Similar results were found by Boulain et al. (2009) when applying an upscaling model using leaf area index for Wankama Millet and Wankama Fallow. It worked well for Wankama fallow, whereas it was less conclusive for Wankama Millet. The main explanation for this difference was low leaf area index in millet fields because of a low density of millet stands due to agricultural practice. There is extensive savanna clearing for food production in the Sahel (Leblanc et al., 2008; Boulain et al., 2009; Cappelaere et al., 2009). To further understand impacts of this land cover change on vegetation production and land-atmosphere exchange processes, there is an urgent need for more study sites covering cropped areas in this region.

In Demokeya, GPP was slightly underestimated for the year 2008 (Fig. 7c) because modelled F_{opt} was much lower than the actual measured value in 2008 (the thick black line in Fig. 4). An improvement of the model could be to incorporate some parameters that constrain or enhance F_{opt} depending on environmental stress. Indeed, the regression tree analysis indicated that incorporating hydrometeorological variables increased the ability to predict both F_{opt} and α. On the other hand, for spatial upscaling purposes, it has been shown that including modelled hydrometeorological constraints on LUE decreases the ability to predict vegetation production due to the incorporated uncertainty in these modelled variables (Fensholt et al., 2006; Ma et al., 2014). For spatial upscaling to regional scales, it is therefore better to simply use relationships to EO data. This is particularly the case for the Sahel, one of the largest dryland areas in the world, which includes only a few sites of hydrometeorological observations.

The pattern seen in the spatially explicit GPP budgets (Fig. 5c) may be influenced by a range of biophysical and anthropogenic factors. The clear North-South gradient is expected given the strong North-South rainfall gradient in the Sahel. The West African Monsoon mentioned above could also be an explanation of high GPP values in the western part of the Sahel, where values were relatively high in relation to GPP at similar latitudes in the central and eastern Sahel (Fig. 5c). The areas with highest GPP are sparsely populated woodlands or shrubby savanna with a relatively dense tree cover (Brandt et al., 2016). However, the maps produced should be used with caution as they are based on upscaling of the only six available EC sites that exist in the region; especially given the issues related to the cropped fields discussed earlier. Still, the average GPP budget for the entire Sahel 2001-2014 was close to an average annual GPP budget as estimated for these six sites (692±89 g C m^{-2} y^{-1}) (Tagesson et al., 2016a). The range of GPP budgets in Fig. 5c is also similar to previous annual GPP budgets reported from other savanna areas across the world (Veenendaal et al., 2004; Chen et al., 2003; Kanniah et al., 2010; Chen et al., 2016).

Although MOD17A2 GPP has previously been shown to capture GPP in several ecosystems types well (Turner et al., 2006; Turner et al., 2005; Heinsch et al., 2006; Sims et al., 2006; Kanniah et al., 2009), it has been shown to underestimate for others (Coops et al., 2007; Gebremichael and Barros, 2006; Sjöström et al., 2013). GPP of Sahelian drylands have not been captured well by MOD17A2 (Sjöström et al., 2013; Fensholt et al., 2006), and as we have shown, this underestimation persists in the latest MOD17A2H GPP (collection 6) product (Fig. 2). The main reason for this pronounced underestimation is that maximum LUE is set to 0.84 g C MJ^{-1} (open shrubland; Demokeya) and 0.86 g C MJ^{-1} (grassland; Agoufou, Dahra, Kelma; Wankama Millet and Wankama Fallow) in the BPLUT, i.e., much lower than maximum LUE measured at the Sahelian measurement sites of this study (average: 2.47 g C MJ^{-1}; range: 1.58-3.50 g C MJ^{-1}) (Sjöström et al., 2013; Tagesson et al., 2015a), a global estimate of ~1.5 g C MJ^{-1} (Garbulsky et al., 2010) and a savanna site in Australia (1.26 g C MJ^{-1}) (Kanniah et al., 2009).

Several dynamic global vegetation models have been used for decades to quantify GPP at different spatial and temporal scales (Dickinson, 1983; Sellers et al., 1997). These models are generally based on the photosynthesis model of Farquhar et al. (1980), a model particularly sensitive to uncertainty in photosynthetic capacity (Zhang et al., 2014). This and several previous studies have shown that both photosynthetic capacity and efficiency (both α and LUE) can vary considerably between seasons as well as spatially, and both within and between vegetation types (Eamus et al., 2013; Garbulsky et al., 2010; Ma et al., 2014; Tagesson et al., 2015a). This variability is difficult to estimate using broad values based on land cover classes, yet most models apply a constant value, which can cause substantial inaccuracies in the estimates of seasonal and spatial variability in GPP. This is particularly a problem in savannas that consists of several plant functional types (C3 and C4 species, and a large variability in tree/herbaceous vegetation fractions) (Scholes and Archer, 1997). This study indicates the ~~strong~~ applicability of EO as a tool for parameterizing spatially explicit estimates of plant physiological variables, which could improve our ability to simulate GPP. Spatially explicit estimates of GPP at a high temporal and spatial resolution are essential for environmental change studies in the Sahel and can contribute to increased knowledge regarding changes in GPP, its relationship to climatic change and anthropogenic forcing, and ~~estimations~~ simulation of ecosystem processes and ~~biochemical and hydrological~~ hydro-biochemical cycles.

Acknowledgements Data is available from Fluxnet (http://fluxnet.ornl.gov) and CarboAfrica (http://www.carboafrica.net/index en.asp). Data for the Mali and Niger sites were made available by the AMMA-CATCH regional observatory (www.amma-catch.org), which is funded by the French Institut de Recherche pour le Développement (IRD) and Institut National des Sciences de l'Univers (INSU). The project was funded by the Danish Council for Independent Research (DFF) Sapere Aude programme. The Faculty of Science, Lund University supported the Dahra and Demokeya measurements with an infrastructure grant. Ardö received support from the Swedish National Space Board.

References

Abdi, A., Seaquist, J., Tenenbaum, D., Eklundh, L., and Ardö, J.: The supply and demand of net primary production in the Sahel, Environ. Res. Lett., 9, 094003, doi:10.1088/1748-9326/9/9/094003, 2014.

Ahlström, A., Raupach, M. R., Schurgers, G., Smith, B., Arneth, A., Jung, M., Reichstein, M., Canadell, J. G., Friedlingstein, P., Jain, A. K., Kato, E., Poulter, B., Sitch, S., Stocker, B. D., Viovy, N., Wang, Y. P., Wiltshire, A., Zaehle, S., and Zeng, N.: The dominant role of semi-arid ecosystems

444 in the trend and variability of the land CO_2 sink, Science, 348, 895-899, 10.1126/science.aaa1668,
445 2015.
446 Baldocchi, D., Falge, E., Gu, L., Olson, R., Hollinger, D., Running, S., Anthoni, P., Bernhofer, C.,
447 Davis, K., Evans, R., Fuentes, J., Goldstein, A., Katul, G., Law, B., Lee, X., Malhi, Y., Meyers, T.,
448 Munger, W., Oechel, W., Paw, K. T., Pilegaard, K., Schmid, H. P., Valentini, R., Verma, S., Vesala,
449 T., Wilson, K., and Wofsy, S.: FLUXNET: A New Tool to Study the Temporal and Spatial
450 Variability of Ecosystem–Scale Carbon Dioxide, Water Vapor, and Energy Flux Densities, Bull.
451 Am. Meteorol. Soc., 82, 2415-2434, 10.1175/1520-0477(2001)082<2415:fantts>2.3.co;2, 2001.
452 Boulain, N., Cappelaere, B., Ramier, D., Issoufou, H. B. A., Halilou, O., Seghieri, J., Guillemin, F.,
453 Oï, M., Gignoux, J., and Timouk, F.: Towards an understanding of coupled physical and biological
454 processes in the cultivated Sahel – 2. Vegetation and carbon dynamics, J. Hydrol., 375, 190-203,
455 10.1016/j.jhydrol.2008.11.045, 2009.
456 Brandt, M., Hiernaux, P., Rasmussen, K., Mbow, C., Kergoat, L., Tagesson, T., Ibrahim, Y. Z.,
457 Wélé, A., Tucker, C. J., and Fensholt, R.: Assessing woody vegetation trends in Sahelian drylands
458 using MODIS based seasonal metrics, Remote Sens. Environ., 183, 215-
459 225, http://dx.doi.org/10.1016/j.rse.2016.05.027, 2016.
460 Broge, N. H., and Leblanc, E.: Comparing prediction power and stability of broadband and
461 hyperspectral vegetation indices for estimation of green leaf area index and canopy chlorophyll
462 density, Remote Sens. Environ., 76, 156-172, http://dx.doi.org/10.1016/S0034-4257(00)00197-8,
463 2001.
464 Cannell, M., and Thornley, J.: Temperature and CO_2 Responses of Leaf and Canopy Photosynthesis:
465 a Clarification using the Non-rectangular Hyperbola Model of Photosynthesis, Ann. Bot., 82, 883-
466 892, 1998.
467 Cappelaere, B., Descroix, L., Lebel, T., Boulain, N., Ramier, D., Laurent, J. P., Favreau, G.,
468 Boubkraoui, S., Boucher, M., Bouzou Moussa, I., Chaffard, V., Hiernaux, P., Issoufou, H. B. A., Le
469 Breton, E., Mamadou, I., Nazoumou, Y., Oi, M., Ottlé, C., and Quantin, G.: The AMMA-CATCH
470 experiment in the cultivated Sahelian area of south-west Niger – Investigating water cycle response
471 to a fluctuating climate and changing environment, J. Hydrol., 375, 34-51,
472 10.1016/j.jhydrol.2009.06.021, 2009.
473 Chen, C., Cleverly, J., and Zhang, L.: Modelling Seasonal and Inter-annual Variations in Carbon
474 and Water Fluxes in an Arid-Zone Acacia Savanna Woodland, 1981–2012, Ecosystems, 19, 625-
475 644, 2016.
476 Chen, X., Hutley, L., and Eamus, D.: Carbon balance of a tropical savanna of northern Australia.,
477 Oecologia, 137, 405-416, 2003.
478 Coops, N. C., Black, T. A., Jassal, R. S., Trofymow, J. A., and Morgenstern, K.: Comparison of
479 MODIS, eddy covariance determined and physiologically modelled gross primary production (GPP)
480 in a Douglas-fir forest stand, Remote Sens. Environ., 107, 385-
481 401, http://dx.doi.org/10.1016/j.rse.2006.09.010, 2007.
482 Dardel, C., Kergoat, L., Hiernaux, P., Mougin, E., Grippa, M., and Tucker, C. J.: Re-greening Sahel:
483 30 years of remote sensing data and field observations (Mali, Niger), Remote Sens. Environ., 140,
484 350-364, http://dx.doi.org/10.1016/j.rse.2013.09.011, 2014.
485 De'ath, G., and Fabricius, K. E.: Classification and regression trees: A powerful yet simple
486 technique for ecological data analysis, Ecology, 81, 3178-3192, 10.2307/177409, 2000.
487 de Ridder, N., Stroosnijder, L., and Cisse, A. M.: Productivity of Sahelian rangelands : a study of
488 the soils, the vegetations and the exploitation of that natural resource, PPS course book. Primary
489 Production in the Sahel, Agricultural University, Wageningen, 1982.
490 Dee, D. P., Uppala, S. M., Simmons, A. J., Berrisford, P., Poli, P., Kobayashi, S., Andrae, U.,
491 Balmaseda, M. A., Balsamo, G., Bauer, P., Bechtold, P., Beljaars, A. C. M., van de Berg, L., Bidlot,

J., Bormann, N., Delsol, C., Dragani, R., Fuentes, M., Geer, A. J., Haimberger, L., Healy, S. B., Hersbach, H., Hólm, E. V., Isaksen, L., Kållberg, P., Köhler, M., Matricardi, M., McNally, A. P., Monge-Sanz, B. M., Morcrette, J. J., Park, B. K., Peubey, C., de Rosnay, P., Tavolato, C., Thépaut, J. N., and Vitart, F.: The ERA-Interim reanalysis: configuration and performance of the data assimilation system, Q. J. Roy. Meteor. Soc., 137, 553-597, 10.1002/qj.828, 2011.

Dickinson, R. E.: Land Surface Processes and Climate—Surface Albedos and Energy Balance, in: Advances in Geophysics, edited by: Barry, S., Elsevier, 305-353, 1983.

Eamus, D., Cleverly, J., Boulain, N., Grant, N., Faux, R., and Villalobos-Vega, R.: Carbon and water fluxes in an arid-zone Acacia savanna woodland: An analyses of seasonal patterns and responses to rainfall events, Agric. For. Meteorol., 182–183, 225-238, http://dx.doi.org/10.1016/j.agrformet.2013.04.020, 2013.

ECMWF: ERA Interim Daily: http://apps.ecmwf.int/datasets/data/interim-full-daily/levtype=sfc/, access: 04-04-2016, 2016a.

ECMWF: ERA-Interim: surface photosynthetically active radiation (surface PAR) values are too low https://software.ecmwf.int/wiki/display/CKB/ERA-Interim%3A+surface+photosynthetically+active+radiation+%28surface+PAR%29+values+are+too+low, access: 7 November, 2016b.

Falge, E., Baldocchi, D., Olson, R., Anthoni, P., Aubinet, M., Bernhofer, C., Burba, G., Ceulemans, R., Clement, R., Dolman, H., Granier, A., Gross, P., Grunwald, T., Hollinger, D., Jensen, N. O., Katul, G., Keronen, P., Kowalski, A., Lai, C. T., Law, B. E., Meyers, T., Moncrieff, J. B., Moors, E., Munger, J. W., Pilegaard, K., Rannik, U., Rebmann, C., Suyker, A., Tenhunen, J., Tu, K., Verma, S., Vesala, T., Wilson, K., and Wofsy, S.: Gap filling strategies for defensible annual sums of net ecosystem exchange, Agric. For. Meteorol., 107, 43-69, 2001.

Farquhar, G. D., Caemmerer, S., and Berry, J. A.: A biochemical model of photosynthetic CO_2 assimilation in leaves of C3 plants, Planta, 149, 78-90, 1980.

Fensholt, R., and Sandholt, I.: Derivation of a shortwave infrared water stress index from MODIS near- and shortwave infrared data in a semiarid environment, Remote Sens. Environ., 87, 111-121, http://dx.doi.org/10.1016/j.rse.2003.07.002, 2003.

Fensholt, R., Sandholt, I., Rasmussen, M. S., Stisen, S., and Diouf, A.: Evaluation of satellite based primary production modelling in the semi-arid Sahel, Remote Sens. Environ., 105, 173-188, 10.1016/j.rse.2006.06.011, 2006.

Fensholt, R., Rasmussen, K., Kaspersen, P., Huber, S., Horion, S., and Swinnen, E.: Assessing Land Degradation/Recovery in the African Sahel from Long-Term Earth Observation Based Primary Productivity and Precipitation Relationships, Remote Sensing, 5, 664-686, 2013.

Garbulsky, M. F., Peñuelas, J., Papale, D., Ardö, J., Goulden, M. L., Kiely, G., Richardson, A. D., Rotenberg, E., Veenendaal, E. M., and Filella, I.: Patterns and controls of the variability of radiation use efficiency and primary productivity across terrestrial ecosystems, Global Ecol. Biogeogr., 19, 253-267, 10.1111/j.1466-8238.2009.00504.x, 2010.

Gates, D. M., Keegan, H. J., Schleter, J. C., and Weidner, V. R.: Spectral Properties of Plants, Appl. Optics, 4, 11-20, 1965.

Gebremichael, M., and Barros, A. P.: Evaluation of MODIS Gross Primary Productivity (GPP) in tropical monsoon regions, Remote Sens. Environ., 100, 150-166, http://dx.doi.org/10.1016/j.rse.2005.10.009, 2006.

Haboudane, D., Miller, J. R., Pattey, E., Zarco-Tejada, P. J., and Strachan, I. B.: Hyperspectral vegetation indices and novel algorithms for predicting green LAI of crop canopies: Modeling and validation in the context of precision agriculture, Remote Sens. Environ., 90, 337-352, http://dx.doi.org/10.1016/j.rse.2003.12.013, 2004.

539 Hanan, N., Kabat, P., Dolman, J., and Elbers, J. A. N.: Photosynthesis and carbon balance of a
540 Sahelian fallow savanna, Global Change Biol., 4, 523-538, 1998.
541 Heinsch, F. A., Maosheng, Z., Running, S. W., Kimball, J. S., Nemani, R. R., Davis, K. J., Bolstad,
542 P. V., Cook, B. D., Desai, A. R., Ricciuto, D. M., Law, B. E., Oechel, W. C., Hyojung, K., Hongyan,
543 L., Wofsy, S. C., Dunn, A. L., Munger, J. W., Baldocchi, D. D., Liukang, X., Hollinger, D. Y.,
544 Richardson, A. D., Stoy, P. C., Siqueira, M. B. S., Monson, R. K., Burns, S. P., and Flanagan, L. B.:
545 Evaluation of remote sensing based terrestrial productivity from MODIS using regional tower eddy
546 flux network observations, IEEE T. Geosci. Remote, 44, 1908-1925, 10.1109/TGRS.2005.853936,
547 2006.
548 Hickler, T., Eklundh, L., Seaquist, J. W., Smith, B., Ardö, J., Olsson, L., Sykes, M. T., and
549 Sjöström, M.: Precipitation controls Sahel greening trend, Geophys. Res. Lett., 32, L21415,
550 doi:10.1029/2005GL024370, 2005.
551 Huber, S., Tagesson, T., and Fensholt, R.: An automated field spectrometer system for studying
552 VIS, NIR and SWIR anisotropy for semi-arid savanna, Remote Sens. Environ., 152, 547–556, 2014.
553 Huete, A., Didan, K., Miura, T., Rodriguez, E. P., Gao, X., and Ferreira, L. G.: Overview of the
554 radiometric and biophysical performance of the MODIS vegetation indices, Remote Sens. Environ.,
555 83, 195–213, 2002.
556 Ide, R., Nakaji, T., and Oguma, H.: Assessment of canopy photosynthetic capacity and estimation
557 of GPP by using spectral vegetation indices and the light-response function in a larch forest, Agric.
558 For. Meteorol., 150, 389-398, 2010.
559 Inoue, Y., Penuelas, J., Miyata, A., and Mano, M.: Normalized difference spectral indices for
560 estimating photosynthetic efficiency and capacity at a canopy scale derived from hyperspectral and
561 CO_2 flux measurements in rice, Remote Sens. Environ., 112, 156-172, 2008.
562 Jin, H., and Eklundh, L.: A physically based vegetation index for improved monitoring of plant
563 phenology, Remote Sens. Environ., 152, 512-525, http://dx.doi.org/10.1016/j.rse.2014.07.010, 2014.
564 Kanniah, K. D., Beringer, J., Hutley, L. B., Tapper, N. J., and Zhu, X.: Evaluation of Collections 4
565 and 5 of the MODIS Gross Primary Productivity product and algorithm improvement at a tropical
566 savanna site in northern Australia, Remote Sens. Environ., 113, 1808-
567 1822, http://dx.doi.org/10.1016/j.rse.2009.04.013, 2009.
568 Kanniah, K. D., Beringer, J., and Hutley, L. B.: The comparative role of key environmental factors
569 in determining savanna productivity and carbon fluxes: A review, with special reference to
570 Northern Australia, Progress in Physical Geography, 34, 459-490, 2010.
571 Kergoat, L., Lafont, S., Arneth, A., Le Dantec, V., and Saugier, B.: Nitrogen controls plant canopy
572 light-use efficiency in temperate and boreal ecosystems, J. Geophys. Res., 113, 1-19,
573 10.1029/2007JG000676, 2008.
574 Leblanc, M. J., Favreau, G., Massuel, S., Tweed, S. O., Loireau, M., and Cappelaere, B.: Land
575 clearance and hydrological change in the Sahel: SW Niger, Global Planet. Change, 61, 135-
576 150, http://dx.doi.org/10.1016/j.gloplacha.2007.08.011, 2008.
577 Levy, P. E., Moncrieff, J. B., Massheder, J. M., Jarvis, P. G., Scott, S. L., and Brouwer, J.: CO2
578 fluxes at leaf and canopy scale in millet, fallow and tiger bush vegetation at the HAPEX-Sahel
579 southern super-site, J. Hydrol., 188, 612-632, http://dx.doi.org/10.1016/S0022-1694(96)03195-2,
580 1997.
581 Ma, X., Huete, A., Yu, Q., Restrepo-Coupe, N., Beringer, J., Hutley, L. B., Kanniah, K. D.,
582 Cleverly, J., and Eamus, D.: Parameterization of an ecosystem light-use-efficiency model for
583 predicting savanna GPP using MODIS EVI, Remote Sens. Environ., 154, 253-
584 271, http://dx.doi.org/10.1016/j.rse.2014.08.025, 2014.
585 Mayaux, P., Bartholomé, E., Massart, M., Cutsem, C. V., Cabral, A., Nonguierma, A., Diallo, O.,
586 Pretorius, C., Thompson, M., Cherlet, M., Pekel, J.-F., Defourny, P., Vasconcelos, M., Gregorio, A.

587 D., S.Fritz, Grandi, G. D., C..Elvidge, P.Vogt, and Belward, A.: EUR 20665 EN –A Land-cover
588 map of Africa, edited by: Centre', E. C. J. R., European Commisions Joint Research Centre,
589 Luxembourg, 38 pp., 2003.
590 Mbow, C., Fensholt, R., Rasmussen, K., and Diop, D.: Can vegetation productivity be derived from
591 greenness in a semi-arid environment? Evidence from ground-based measurements, J. Arid
592 Environ., 97, 56-65, http://dx.doi.org/10.1016/j.jaridenv.2013.05.011, 2013.
593 Merbold, L., Ardö, J., Arneth, A., Scholes, R. J., Nouvellon, Y., de Grandcourt, A., Archibald, S.,
594 Bonnefond, J. M., Boulain, N., Brueggemann, N., Bruemmer, C., Cappelaere, B., Ceschia, E., El-
595 Khidir, H. A. M., El-Tahir, B. A., Falk, U., Lloyd, J., Kergoat, L., Le Dantec, V., Mougin, E.,
596 Muchinda, M., Mukelabai, M. M., Ramier, D., Roupsard, O., Timouk, F., Veenendaal, E. M., and
597 Kutsch, W. L.: Precipitation as driver of carbon fluxes in 11 African ecosystems, Biogeosciences, 6,
598 1027-1041, 10.5194/bg-6-1027-2009, 2009.
599 Moncrieff, J. B., Monteny, B., Verhoef, A., Friborg, T., Elbers, J., Kabat, P., de Bruin, H., Soegaard,
600 H., Jarvis, P. G., and Taupin, J. D.: Spatial and temporal variations in net carbon flux during
601 HAPEX-Sahel, J. Hydrol., 188–189, 563-588, 10.1016/s0022-1694(96)03193-9, 1997.
602 Monteith, J. L.: Solar radiation and productivity in tropical ecosystems, J. Appl. Ecol., 9, 747-766,
603 1972.
604 Monteith, J. L.: Climate and the efficiency of crop production in Britain, Philos. Trans. Roy. Soc. B.,
605 281, 277-294, 1977.
606 Monteny, B. A., Lhomme, J. P., Chehbouni, A., Troufleau, D., Amadou, M., Sicot, M., Verhoef, A.,
607 Galle, S., Said, F., and Lloyd, C. R.: The role of the Sahelian biosphere on the water and the CO2
608 cycle during the HAPEX-Sahel experiment, J. Hydrol., 188, 516-
609 535, http://dx.doi.org/10.1016/S0022-1694(96)03191-5, 1997.
610 Mutanga, O., and Skidmore, A. K.: Narrow band vegetation indices overcome the saturation
611 problem in biomass estimation, Int. J. Remote Sens., 25, 3999-4014,
612 10.1080/01431160310001654923, 2004.
613 NASA: Reverb ECHO: http://reverb.echo.nasa.gov/reverb/, access: June 2016, 2016.
614 Papale, D., Reichstein, M., Aubinet, M., Canfora, E., Bernhofer, C., Kutsch, W., Longdoz, B.,
615 Rambal, S., Valentini, R., Vesala, T., and Yakir, D.: Towards a standardized processing of Net
616 Ecosystem Exchange measured with eddy covariance technique: algorithms and uncertainty
617 estimation, Biogeosciences, 3, 571-583, 10.5194/bg-3-571-2006, 2006.
618 Paruelo, J. M., Garbulsky, M. F., Guerschman, J. P., and Jobbágy, E. G.: Two decades of
619 Normalized Difference Vegetation Index changes in South America: identifying the imprint of
620 global change, Int. J. Remote Sens., 25, 2793-2806, 10.1080/01431160310001619526, 2004.
621 Poulter, B., Frank, D., Ciais, P., Myneni, R. B., Andela, N., Bi, J., Broquet, G., Canadell, J. G.,
622 Chevallier, F., Liu, Y. Y., Running, S. W., Sitch, S., and van der Werf, G. R.: Contribution of semi-
623 arid ecosystems to interannual variability of the global carbon cycle, Nature, 509, 600-603,
624 10.1038/nature13376, 2014.
625 Prince, S. D., Kerr, Y. H., Goutorbe, J. P., Lebel, T., Tinga, A., Bessemoulin, P., Brouwer, J.,
626 Dolman, A. J., Engman, E. T., Gash, J. H. C., Hoepffner, M., Kabat, P., Monteny, B., Said, F.,
627 Sellers, P., and Wallace, J.: Geographical, biological and remote sensing aspects of the hydrologic
628 atmospheric pilot experiment in the sahel (HAPEX-Sahel), Remote Sens. Environ., 51, 215-
629 234, http://dx.doi.org/10.1016/0034-4257(94)00076-Y, 1995.
630 Qi, J., Chehbouni, A., Huete, A. R., Kerr, Y. H., and Sorooshian, S.: A modified soil adjusted
631 vegetation index, Remote Sens. Environ., 48, 119-126, 1994.
632 Richter, K., Atzberger, C., Hank, T. B., and Mauser, W.: Derivation of biophysical variables from
633 Earth observation data: validation and statistical measures, J. Appl. Remote Sens., 6, 063557,
634 10.1117/1.JRS.6.063557, 2012.

635 Rietkerk, M., Ketner, P., Stroosnijder, L., and Prins, H. H. T.: Sahelian rangeland development; a
636 catastrophe?, J. Range Manage., 49, 512-519, 1996.
637 Rockström, J., and de Rouw, A.: Water, nutrients and slope position in on-farm pearl millet
638 cultivation in the Sahel, Plant Soil, 195, 311-327, 10.1023/A:1004233303066, 1997.
639 Roujean, J.-L., and Breon, F.-M.: Estimating PAR absorbed by vegetation from bidirectional
640 reflectance measurements, Remote Sens. Environ., 51, 375-384, http://dx.doi.org/10.1016/0034-
641 4257(94)00114-3, 1995.
642 Rouse, J. W., Haas, R. H., Schell, J. A., Deering, D. W., and Harlan, J. C.: Monitoring the Vernal
643 Advancement of Retrogradation of Natural Vegetation, Type III, Final Report, Greenbelt, MD,
644 1974.
645 Ruimy, A., Saugier, B., and Dedieu, G.: Methodology for the estimation of terrestrial net primary
646 production from remotely sensed data., J. Geophys. Res., 99, 5263-5283., 1994.
647 Running, S. W., Nemani, R. R., Heinsch, F. A., Zhao, M., Reeves, M., and Hashimoto, H.: A
648 Continuous Satellite-Derived Measure of Global Terrestrial Primary Production, BioScience, 54,
649 547-560, 10.1641/0006-3568(2004)054[0547:ACSMOG]2.0.CO;2, 2004.
650 Running, S. W., and Zhao, M.: User's Guide. Daily GPP and Annual NPP (MOD17A2/A3)
651 Products NASA Earth Observing System MODIS Land Algorithm. Version 3.0 For Collection 6.,
652 University of Montana, USA, NASA, 2015.
653 Scholes, R. J., and Archer, S. R.: Tree-grass interactions in savannas, Annual Review of Ecology
654 and Systematics, 28, 517-544, 1997.
655 Sellers, P. J., Dickinson, R. E., Randall, D. A., Betts, A. K., Hall, F. G., Berry, J. A., Collatz, G. J.,
656 Denning, A. S., Mooney, H. A., Nobre, C. A., Sato, N., Field, C. B., and Henderson-Sellers, A.:
657 Modeling the Exchanges of Energy, Water, and Carbon Between Continents and the Atmosphere,
658 Science, 275, 502-509, 10.1126/science.275.5299.502, 1997.
659 Sims, D. A., Rahman, A. F., Cordova, V. D., El-Masri, B. Z., Baldocchi, D. D., Flanagan, L. B.,
660 Goldstein, A. H., Hollinger, D. Y., Misson, L., Monson, R. K., Oechel, W. C., Schmid, H. P.,
661 Wofsy, S. C., and Xu, L.: On the use of MODIS EVI to assess gross primary productivity of North
662 American ecosystems, J. Geophys. Res., 111, G04015, 10.1029/2006JG000162, 2006.
663 Sjöström, M., Ardö, J., Eklundh, L., El-Tahir, B. A., El-Khidir, H. A. M., Hellström, M., Pilesjö, P.,
664 and Seaquist, J.: Evaluation of satellite based indices for gross primary production estimates in a
665 sparse savanna in the Sudan, Biogeosciences, 6, 129-138, 2009.
666 Sjöström, M., Zhao, M., Archibald, S., Arneth, A., Cappelaere, B., Falk, U., de Grandcourt, A.,
667 Hanan, N., Kergoat, L., Kutsch, W., Merbold, L., Mougin, E., Nickless, A., Nouvellon, Y., Scholes,
668 R. J., Veenendaal, E. M., and Ardö, J.: Evaluation of MODIS gross primary productivity for Africa
669 using eddy covariance data, Remote Sens. Environ., 131, 275-
670 286, http://dx.doi.org/10.1016/j.rse.2012.12.023, 2013.
671 Tagesson, T., Eklundh, L., and Lindroth, A.: Applicability of leaf area index products for boreal
672 regions of Sweden, Int. J. Remote Sens., 30, 5619–5632, 2009.
673 Tagesson, T., Fensholt, R., Cropley, F., Guiro, I., Horion, S., Ehammer, A., and Ardö, J.: Dynamics
674 in carbon exchange fluxes for a grazed semi-arid savanna ecosystem in West Africa, Agr. Ecosyst.
675 Environ., 205, 15-24, http://dx.doi.org/10.1016/j.agee.2015.02.017, 2015a.
676 Tagesson, T., Fensholt, R., Guiro, I., Rasmussen, M. O., Huber, S., Mbow, C., Garcia, M., Horion,
677 S., Sandholt, I., Rasmussen, B. H., Göttsche, F. M., Ridler, M.-E., Olén, N., Olsen, J. L., Ehammer,
678 A., Madsen, M., Olesen, F. S., and Ardö, J.: Ecosystem properties of semi-arid savanna grassland in
679 West Africa and its relationship to environmental variability, Global Change Biol., 21, 250-264, doi:
680 10.1111/gcb.12734, 2015b.

Tagesson, T., Fensholt, R., Huber, S., Horion, S., Guiro, I., Ehammer, A., and Ardö, J.: Deriving seasonal dynamics in ecosystem properties of semi-arid savannas using in situ based hyperspectral reflectance, Biogeosciences, 12, 4621-4635, doi:10.5194/bg-12-4621-2015, 2015c.
Tagesson, T., Fensholt, R., Cappelaere, B., E., M., Horion, S., L., K., Nieto, H., Ehammer, A., Demarty, J., and Ardö, J.: Spatiotemporal variability in carbon exchange fluxes across the Sahel Agric. For. Meteorol., 226–227, 108-118, 2016a.
Tagesson, T., Fensholt, R., Guiro, I., Cropley, F., Horion, S., Ehammer, A., and Ardö, J.: Very high carbon exchange fluxes for a grazed semi-arid savanna ecosystem in West Africa, Danish Journal of Geography, 116, 93-109, http://dx.doi.org/10.1080/00167223.2016.1178072 2016b.
Timouk, F., Kergoat, L., Mougin, E., Lloyd, C. R., Ceschia, E., Cohard, J. M., Rosnay, P. d., Hiernaux, P., Demarez, V., and Taylor, C. M.: Response of surface energy balance to water regime and vegetation development in a Sahelian landscape, J. Hydrol., 375, 12-12, 10.1016/j.jhydrol.2009.04.022, 2009.
Turner, D. P., Ritts, W. D., Cohen, W. B., Maeirsperger, T. K., Gower, S. T., Kirschbaum, A. A., Running, S. W., Zhao, M., Wofsy, S. C., Dunn, A. L., Law, B. E., Campbell, J. L., Oechel, W. C., Kwon, H. J., Meyers, T. P., Small, E. E., Kurc, S. A., and Gamon, J. A.: Site-level evaluation of satellite-based global terrestrial gross primary production and net primary production monitoring, Global Change Biol., 11, 666-684, 2005.
Turner, D. P., Ritts, W. D., and Cohen, W. B.: Evaluation of MODIS NPP and GPP products across multiple biomes, Remote Sens. Environ., 102, 282-293, 2006.
United Nations: Sahel Regional Strategy Mid-Year Review 2013 New York, 1-59, 2013.
Veenendaal, E. M., Kolle, O., and Lloyd, J.: Seasonal variation in energy fluxes and carbon dioxide exchange for a broadleaved semi-arid savanna (Mopane woodland) in Southern Africa, Global Change Biol., 10, 318-328, 2004.
Velluet, C., Demarty, J., Cappelaere, B., Braud, I., Issoufou, H. B. A., Boulain, N., Ramier, D., Mainassara, I., Charvet, G., Boucher, M., Chazarin, J. P., Oï, M., Yahou, H., Maidaji, B., Arpin-Pont, F., Benarrosh, N., Mahamane, A., Nazoumou, Y., Favreau, G., and Seghieri, J.: Building a field- and model-based climatology of local water and energy cycles in the cultivated Sahel; annual budgets and seasonality, Hydrol. Earth Syst. Sci., 18, 5001-5024, 10.5194/hess-18-5001-2014, 2014.
Yoder, B. J., and Pettigrew-Crosby, R. E.: Predicting nitrogen and chlorophyll content and concentrations from reflectance spectra (400–2500 nm) at leaf and canopy scales, Remote Sens. Environ., 53, 199-211, http://dx.doi.org/10.1016/0034-4257(95)00135-N, 1995.
Zhang, Y., Guanter, L., Berry, J. A., Joiner, J., van der Tol, C., Huete, A., Gitelson, A., Voigt, M., and Köhler, P.: Estimation of vegetation photosynthetic capacity from space-based measurements of chlorophyll fluorescence for terrestrial biosphere models, Global Change Biol., 20, 3727-3742, 10.1111/gcb.12664, 2014.

Tables

Table 1. Description of the six measurement sites including location, soil type, ecosystem type and dominant species.

Measurement site	Coordinates	Soil type	Ecosystem	Dominant species
Agoufou[a] (ML-AgG, Mali)	15.34°N, 1.48°W	Sandy ferruginous Arenosol	Open woody savannah (4% tree cover)	Trees: *Acacia spp., Balanites aegyptiaca, Combretum glutinosum* Herbs: *Zornia glochidiata, Cenchrus biflorus, Aristida mutabilis, Tragus berteronianus*
Dahra[b] (SN-Dah, Senegal)	15.40°N, 15.43°W	Sandy luvic arenosol	Grassland/shrubland Savanna (3% tree cover)	Trees: *Acacia spp., Balanites aegyptiaca* Herbs: *Zornia latifolia, Aristida adscensionis, Cenchrus biflorus*
Demokeya[c] (SD-Dem, Sudan)	13.28°N, 30.48°E	Cambic Arenosol	Sparse acacia savannah (7% tree cover)	*Trees: Acacia spp.,* Herbs: *Aristida pallida, Eragrostis tremula, Cenchrus biflorus*
Kelma[a] (ML-Kem, Mali)	15.22°N, 1.57°W	Clay soil depression	Open acacia forest (90% tree cover)	Trees: *Acacia seyal, Acacia nilotica, Balanites aegyptiaca* Herbs: *Sporobolus hevolvus, Echinochloa colona, Aeschinomene sensitive*
Wankama Fallow[d] (NE-WaF, Niger)	13.65°N, 2.63°E	Sandy ferruginous Arenosol	Fallow bush	*Guiera senegalensis*
Wankama Millet[e] (NE-WaM, Niger)	13.64°N, 2.63°E	Sandy ferruginous Arenosol	Millet crop	*Pennisetum glaucum*

[a](Timouk et al., 2009)
[b](Tagesson et al., 2015b)
[c](Sjöström et al., 2009)
[d](Velluet et al., 2014)
[e](Boulain et al., 2009)

Table 2. Correlation between intra-annual dynamics in photosynthetic capacity (F_{opt}; F_{opt_frac} for all sites), quantum efficiency (α; $\alpha_{\_frac}$ for all sites) and the different vegetation indices for the six measurement sites (Fig. 1). Values are averages±1 standard deviation from 200 bootstrapping runs. The bold values are the indices with the strongest correlation. EVI is the enhanced vegetation index, NDVI is the normalized difference vegetation index, RDVI is the renormalized difference vegetation index, SIWSI is the shortwave infrared water stress index. $SIWSI_{12}$ is based on the MODIS Bidirectional Reflectance Distribution Functions (NBAR) band 2 and band 5, whereas $SIWSI_{16}$ is based on MODIS NBAR band 2 and band 6.

Measurement site	F_{opt}					α				
	EVI	NDVI	RDVI	$SIWSI_{12}$	$SIWSI_{16}$	EVI	NDVI	RDVI	$SIWSI_{12}$	SIW
ML-AgG	0.89±0.02	0.87±0.02	0.95±0.01	**-0.95±0.01**	-0.93±0.02	0.92±0.02	0.91±0.01	**0.96±0.01**	-0.94±0.01	-0.88
SN-Dah	0.92±0.005	0.91±0.01	0.96±0.003	**-0.96±0.004**	-0.93±0.01	0.89±0.01	0.90±0.01	**0.93±0.01**	-0.92±0.01	-0.87
SD-Dem	0.81±0.01	0.78±0.01	0.91±0.01	**-0.93±0.01**	-0.90±0.01	0.76±0.02	0.73±0.02	**0.86±0.01**	-0.82±0.02	-0.79
MA-Kem	0.77±0.02	0.83±0.02	0.95±0.01	**-0.95±0.01**	-0.90±0.02	0.69±0.05	0.73±0.04	**0.80±0.03**	-0.77±0.03	-0.76
NE-WaF	0.87±0.02	0.81±0.02	0.78±0.02	**-0.90±0.01**	-0.80±0.02	**0.89±0.01**	0.84±0.01	0.85±0.01	-0.88±0.01	-0.79
NE-WaM	0.41±0.05	0.50±0.04	**0.72±0.03**	-0.55±0.04	-0.43±0.05	0.72±0.02	0.76±0.02	**0.81±0.01**	-0.75±0.01	-0.72
All sites	0.86±0.0	0.79±0.0	**0.90±0.0**	0.75±0.0	0.70±0.0	0.83±0.01	0.80±0.01	**0.86±0.01**	0.62±0.01	0.54

Table 3. Statistics for the regression tree analysis. The regression tree analysis was used to study relationships between intra-annual dynamics in the photosynthetic capacity (F_{opt}; F_{opt_frac} for all sites) and quantum efficiency (α; $\alpha_{\_frac}$ for all sites) and the explanatory variables ~~for the six measurement sites~~ (Fig. 1). The pruning level is the number of splits of the regression tree and an indication of complexity of the system.

Measurement site	Explanatory variables:					Pruning level	R^2
F_{opt}	1	2	3	4	5		
ML-AgG	$SIWSI_{12}$	Tair	PAR	SWC		16	0.98
SN-Dah	$SIWSI_{12}$	SWC	VPD	Tair	PAR	84	0.98
SD-Dem	$SIWSI_{12}$	VPD	SWC	Tair	PAR	33	0.97
ML-Kem	$SIWSI_{12}$	PAR	Tair	VPD		22	0.98
NE-WaF	$SIWSI_{12}$	SWC	VPD	Tair		14	0.92
NE-WaM	RDVI	SWC	VPD	Tair		18	0.75
All sites	RDVI	SWC	Tair	VPD		16	0.87
α							
ML-AgG	RDVI					3	0.95
SN-Dah	RDVI	VPD	SWC	Tair	PAR	21	0.93
SD-Dem	RDVI	SWC	PAR	Tair		16	0.93
ML-Kem	RDVI	Tair				4	0.75
NE-WaF	EVI	SWC	VPD			10	0.90
NE-WaM	RDVI	SWC	VPD	Tair		15	0.86
All sites	RDVI	SWC	VPD	Tair		16	0.84

Table 4. Annual peak values of quantum efficiency (α_{peak}; μmol CO_2 μmol PAR^{-1}) and photosynthetic capacity (F_{opt_peak}; μmol CO_2 m^{-2} s^{-1}) for the six measurement sites (Fig. 1). The peak values are the 2-week running mean with highest annual value.

Measurement site	Year	α_{peak}	$F_{opt\ peak}$
ML-AgG	2007	0.0396	24.5
SN-Dah	2010	0.0638	50.0
	2011	0.0507	42.3
	2012	0.0480	39.2
	2013	0.0549	40.0
SD-Dem	2007	0.0257	16.5
	2008	0.0327	21.0
	2009	0.0368	16.5
ML-Kem	2007	0.0526	33.5
NE-WaF	2005	0.0273	18.2
	2006	0.0413	21.0
NE-WaM	2005	0.0252	10.6
	2006	0.0200	10.1
Average		0.0399	26.4

Table 5. Correlation matrix between annual peak values of photosynthetic capacity (F_{opt_peak}) and quantum efficiency (α_{peak}) and measured environmental variables. P is annual rainfall; T_{air} is yearly averaged air temperature at 2-m height; SWC is yearly averaged soil water content (% volumetric water content) measured at 0.1 m depth; Rh is yearly averaged relative humidity; VPD is yearly averaged vapour pressure deficit; R_g is yearly averaged incoming global radiation; N and C cont. are soil nitrogen and carbon contents; $NDVI_{peak}$ is annual peak normalized difference vegetation index (NDVI); EVI_{peak} is annual peak enhanced vegetation index (EVI); $RDVI_{peak}$ is annual peak renormalized difference vegetation index (RDVI); $SIWSI_{12peak}$ is annual peak short-wave infrared water stress index based on MODIS NBAR band 2 and band 5; and $SIWSI_{16peak}$ is annual peak short-wave infrared water stress index based on MODIS NBAR band 2 and band 6. Sample size was 13 for all except the marked explanatory variables.

Explanatory variable	F_{opt_peak}	α_{peak}
Meteorological data		
P (mm)	0.24±0.26	0.13±0.27
T_{air} (°C)	-0.07±0.25	-0.01±0.25
SWC (%)[a]	0.33±0.25	0.16±0.27
Rh (%)	0.73±0.16*	0.60±0.19
VPD (hPa)	0.20±0.26	0.15±0.30
R_g (W m^{-2})	-0.48±0.21	-0.41±0.24
Biomass and edaphic data		
Biomass (g DW m^{-2})[a]	0.77±0.15*	0.74±0.14*
C3/C4 ratio	-0.05±0.26	0.06±0.30
N cont. (%)[b]	0.22±0.11	0.35±0.14
C cont. (%)[b]	0.89±0.06**	0.87±0.07**
Earth observation data		
$NDVI_{peak}$	0.94±0.05**	0.87±0.07**
EVI_{peak}	0.93±0.04**	0.87±0.07**
$RDVI_{peak}$	0.93±0.04**	0.89±0.07**
$SIWSI_{12peak}$	0.85±0.08**	0.84±0.08**
$SIWSI_{16peak}$	0.67±0.12*	0.65±0.15*
Photosynthetic variables		
F_{opt}	-	0.94±0.03**

[a]sample size equals 11.
[b]sample size equals 9.
* significant at 0.05 level.
** significant at 0.01 level

Table 6. Statistics regarding the evaluation of the gross primary production (GPP) model for the six measurement sites (Fig. 1). In situ and modelled GPP are averages ± 1 standard deviation. RMSE is the root mean square error, and slope, intercept and R^2 are from the fitted ordinary least squares linear regression.

Measurement site	In situ GPP (μmol CO_2 m^{-2} s^{-1})	Modelled GPP (μmol CO_2 m^{-2} s^{-1})	RMSE (μmol CO_2 m^{-2} s^{-1})	slope	Intercept (μmol CO_2 m^{-2} s^{-1})	R^2
ML-AgG	5.35±6.38	5.97±5.80	2.48±0.10	0.84±0.003	1.46±0.01	0.86±0.002
SN-Dah	9.39±10.17	8.87±9.67	3.99±1.34	0.88±0.002	0.62±0.01	0.85±0.001
SD-Dem	4.26±4.55	3.98±3.90	3.15±1.06	0.63±0.003	1.31±0.007	0.54±0.02
ML-Kem	11.16±8.02	10.52±9.22	4.35±1.23	1.02±0.003	-0.82±0.03	0.78±0.002
NE-WaF	5.77±4.17	6.63±3.53	2.47±1.05	0.70±0.005	2.58±0.02	0.69±0.003
NE-WaM	3.04±1.93	6.35±3.47	4.12±0.99	1.31±0.004	2.37±0.02	0.53±0.003
Average	6.73±7.72	7.02±7.39	3.68±0.55	0.83±0.07	1.34±0.82	0.84±0.07

Table 7. The parameters for Eq. 13 that were used in the final gross primary production (GPP) model. RMSE is the root mean square error, and R^2 is the coefficient of determination for the regression models predicting the different variables.

Parameter	Value	RMSE	R^2
k_{Fopt}	79.6±6.3	5.1±1.3	0.89±0.05
m_{Fopt}	-7.3±3.2		
l_{Fopt}	3.51±0.19	0.15±0.02	0.88±0.06
n_{Fopt}	0.03±0.006		
α	0.16±0.02	0.0069±0.0021	0.81±0.10
m_{α}	-0.014±0.007		
l_{α}	3.75±0.27	0.20±0.02	0.80±0.10
n_{α}	0.02±0.007		

Figures

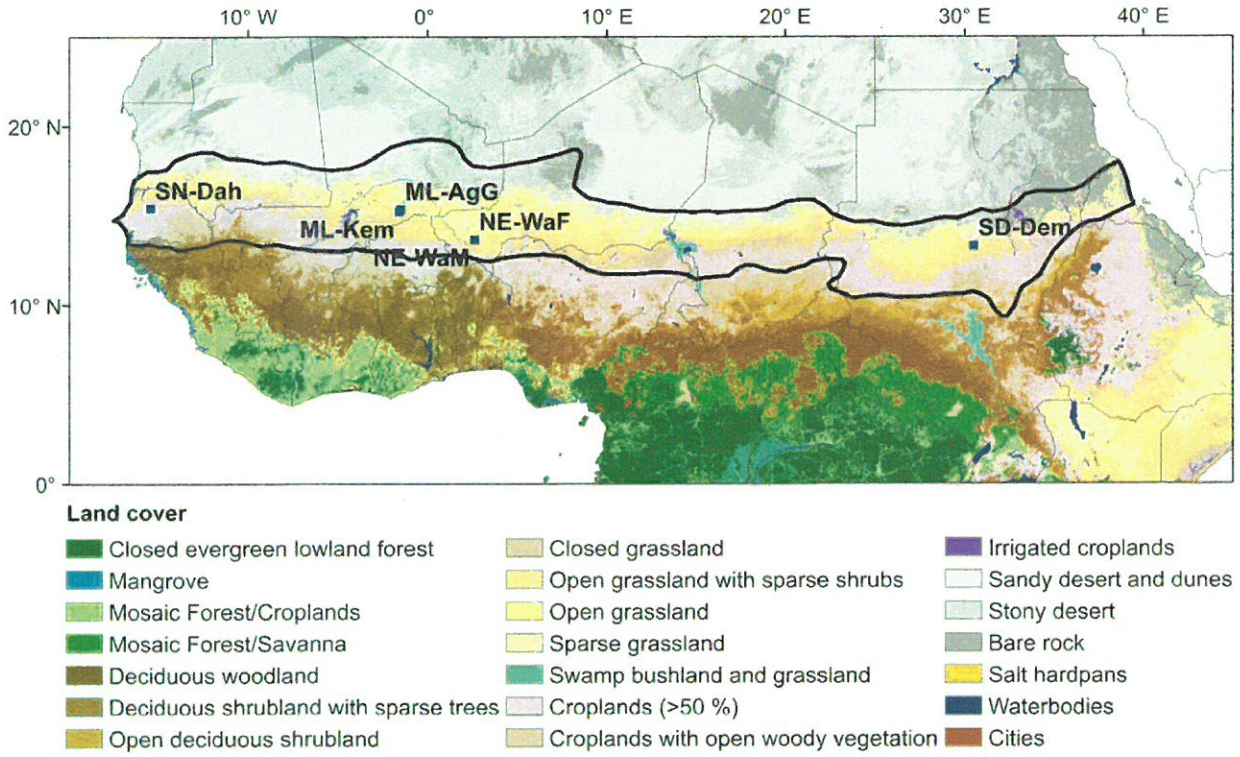

Figure 1. Land cover classes for the Sahel and the location of the six measurement sites ~~included in the~~ study. The land cover classes are based on multi-sensor satellite observations (Mayaux et al., 2003). The sites are Agoufou (ML-AgG), Dahra (SN-Dah), Demokeya (SD-Dem), Kelma (ML-Kem), Wankama Fallow (NE-WaF) and Wankama Millet (NE-WaM). The thick black line ~~are the~~ borders of the Sahel based on the ~~isohytes~~ 150 and 700 mm ~~of annual precipitation~~ (Prince et al., 1995).

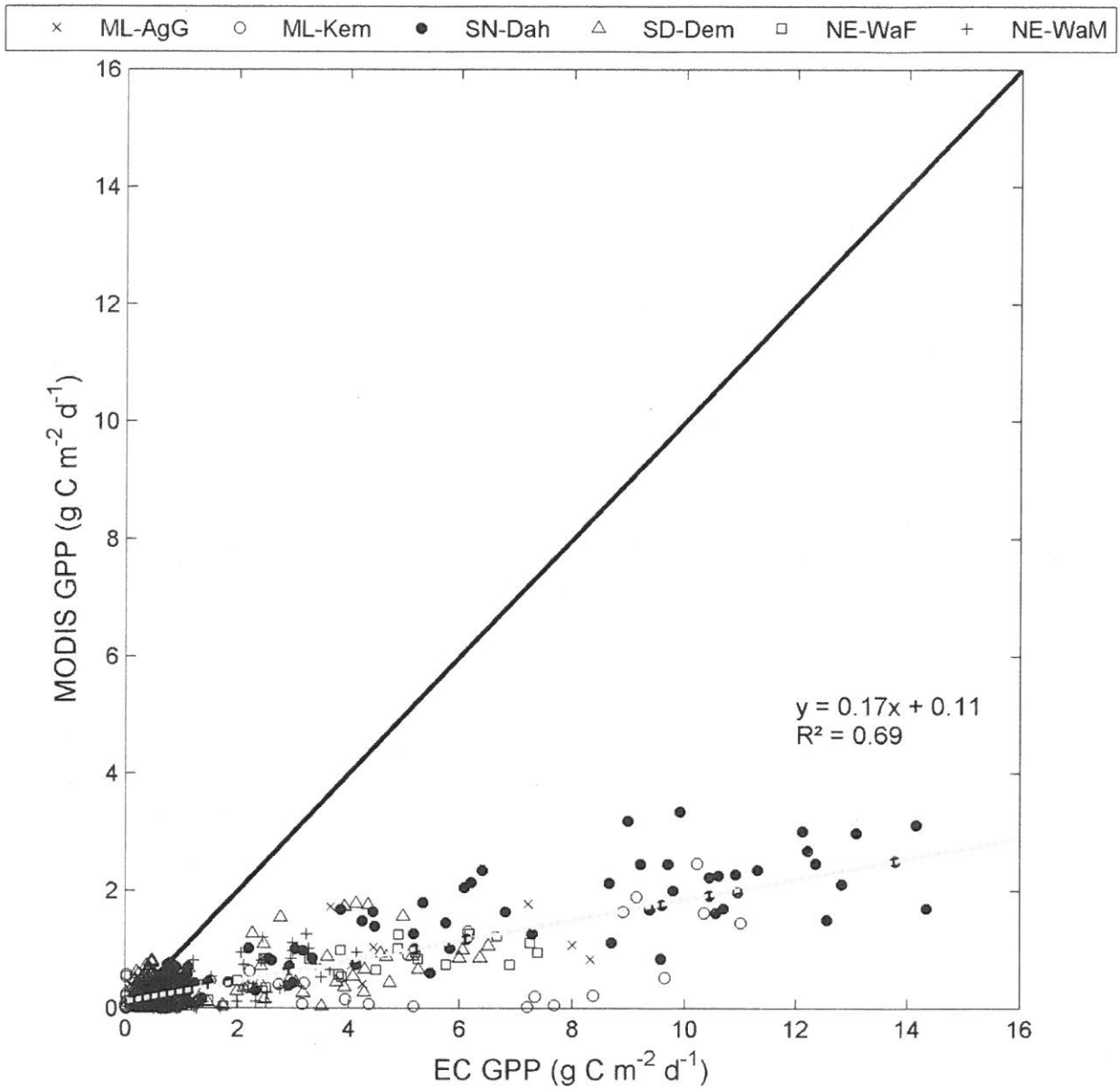

Figure 2. Evaluation of the MODIS based GPP product MOD17A2H (collection 6) against eddy covariance based GPP from the six measurement sites (Fig. 1) across the Sahel. The thick black line shows the one-to-one ratio and the grey dotted line is the fitted ordinary least squares ~~linear~~ regression.

5

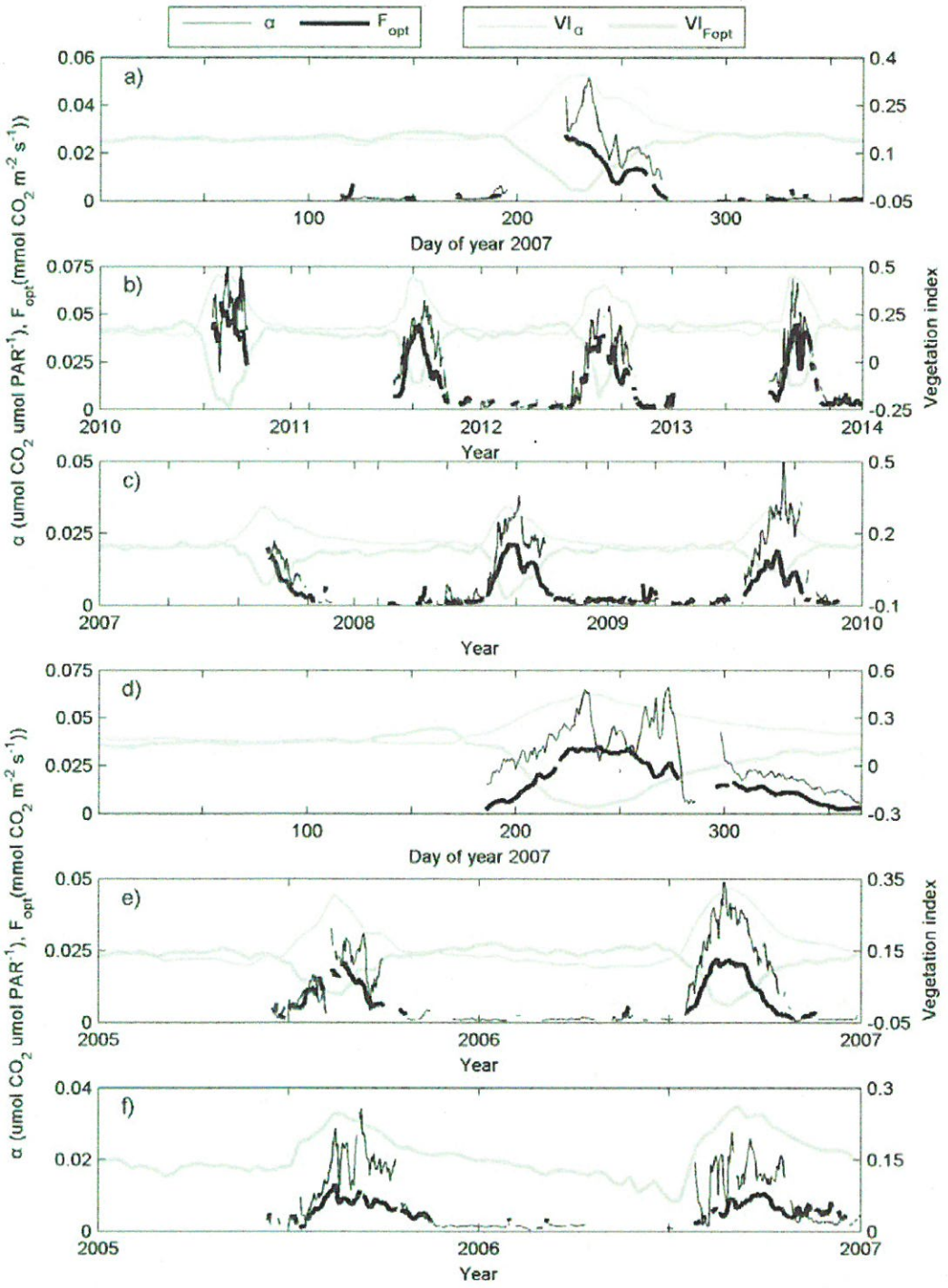
α
F_{opt}
VI_{α}
VI_{Fopt}
a)
b)
c)
d)
e)
f)
α (umol CO_2 umol PAR^{-1}), F_{opt}(mmol CO_2 m^{-2} s^{-1}))
Vegetation index
Day of year 2007
Year

Time series of

Figure 3. ~~Dynamics~~ of photosynthetic capacity (F_{opt}) and quantum efficiency (α) for the six measurement sites. Also included are ~~dynamics in the~~ vegetation indices with highest correlation ~~to the intra-annual dynamics~~ with F_{opt} (VI_{Fopt}) and quantum efficiency (VI_{α}) (Table 2). The sites are a) Agoufou (ML-AgG), b) Dahra (SN-Dah), c) Demokeya (SD-Dem), d) Kelma (ML-Kem), e) Wankama Fallow (NE-WaF) and f) Wankama Millet (NE-WaM).

timeseries of the

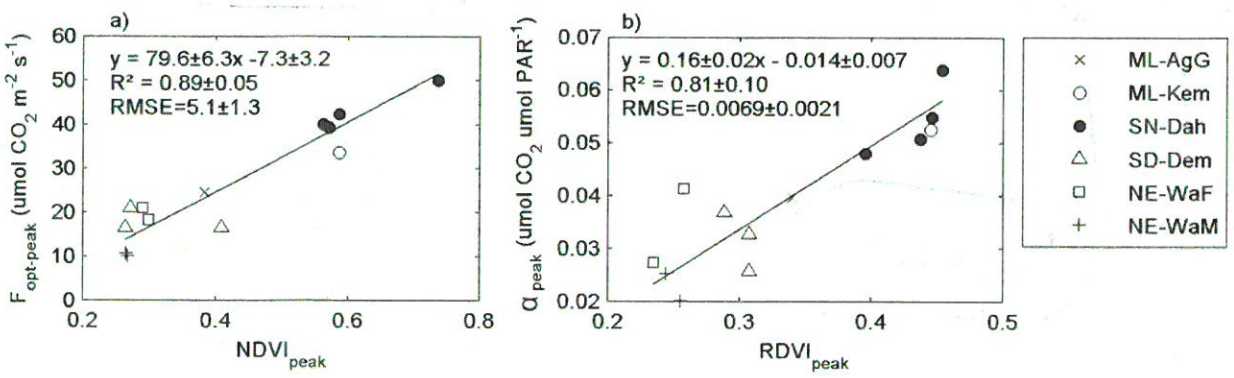

Figure 4. Scatter plots of annual peak values for the six measurement sites (Fig. 1) of a) photosynthetic capacity (F_{opt_peak}) and b) quantum efficiency (α_{peak}) against peak values of normalized difference vegetation index ($NDVI_{peak}$) and renormalized difference vegetation index ($RDVI_{peak}$), respectively. The annual peak values were estimated by taking the annual maximum of a 2-week running mean.

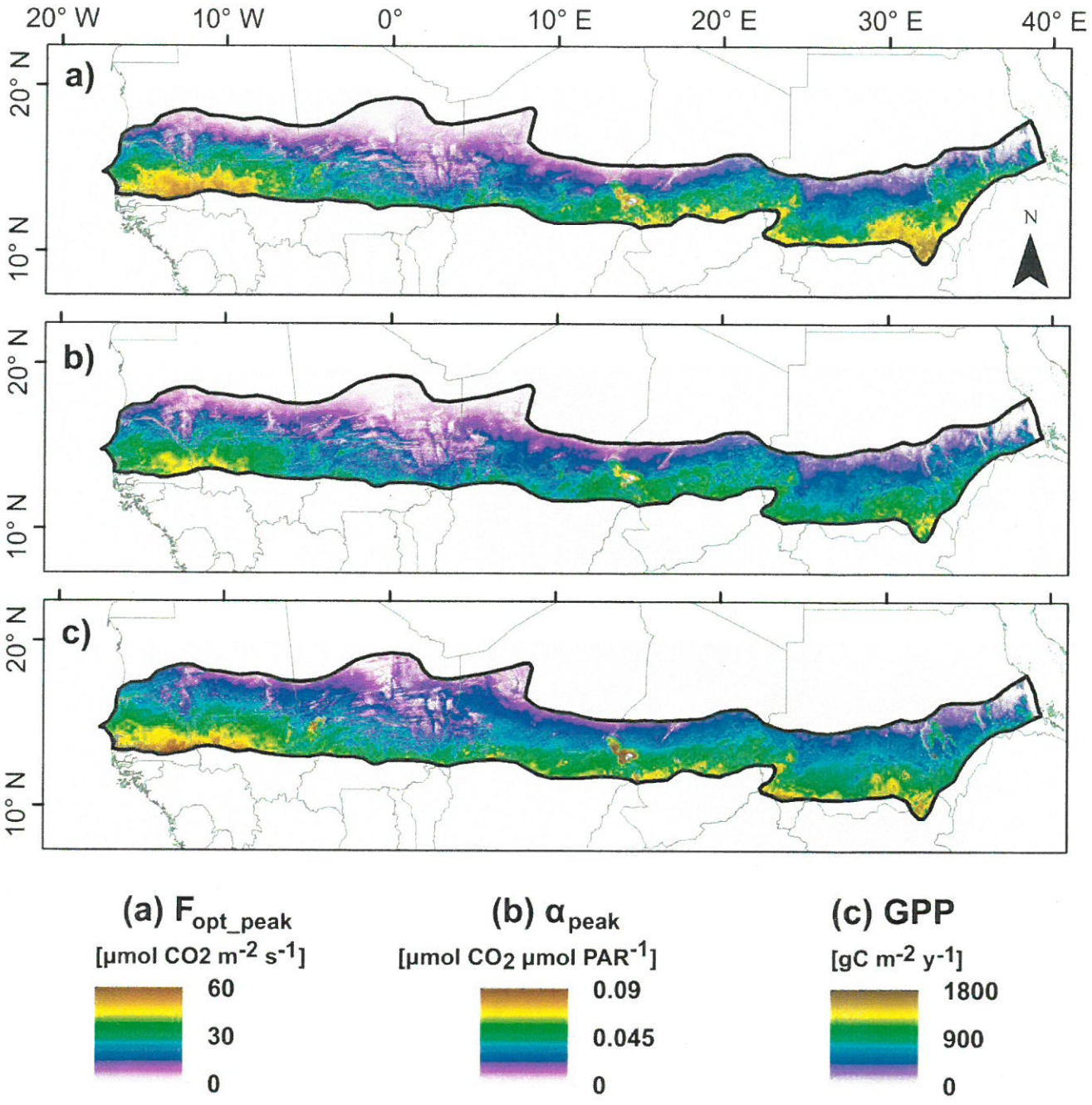

Figure 5. Maps of a) peak values of photosynthetic capacity (F_{opt_peak}) averaged for 2001-2014, b) peak values of quantum efficiency (α_{peak}) averaged for 2001-2014, and c) annual budgets of GPP averaged for 2001-2014.

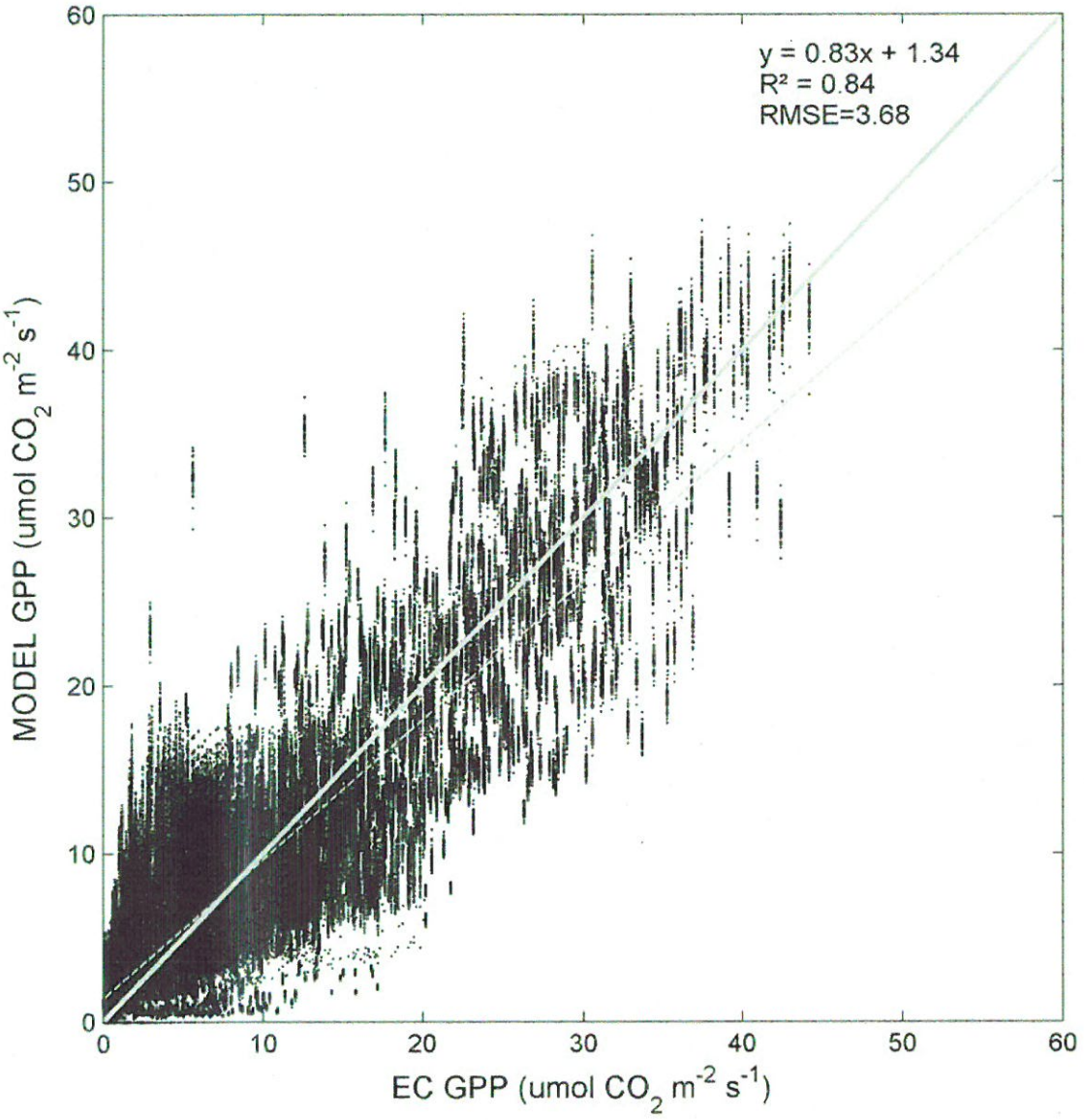

Figure 6. Evaluation of the modelled gross primary production (GPP) (Eq. 13) against in situ GPP from all six measurement sites across the Sahel. The thick grey line shows the one-to-one ratio, whereas the thin dotted grey line is the fitted ordinary least squares linear regression.

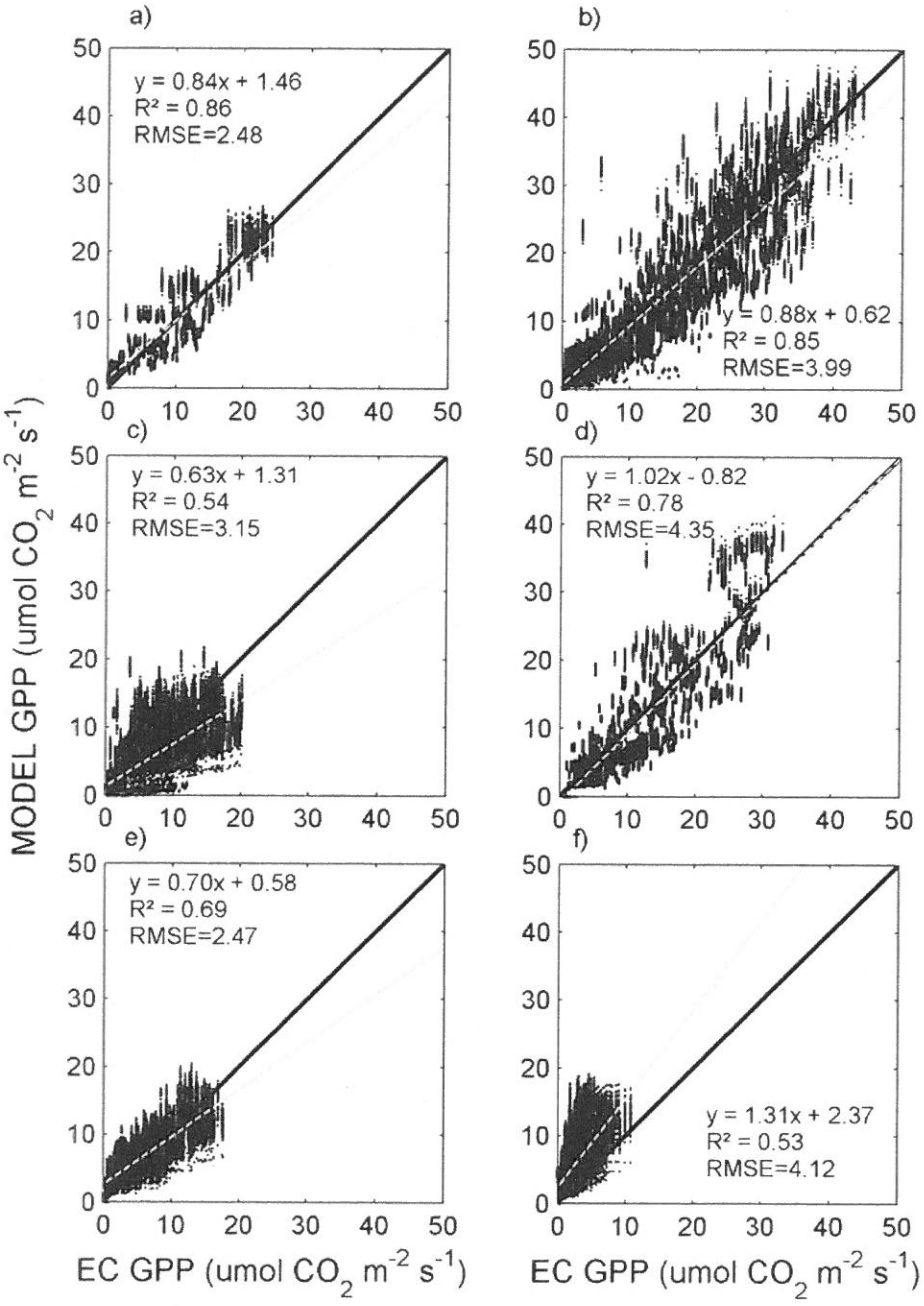

Figure 7. Evaluation of the modelled gross primary production (GPP) (Eq. 13) against in situ GPP for the six sites ~~across~~ Sahel (Fig. 1). The thick black line shows the one-to-one ratio, whereas the dotted thin grey line is the fitted ordinary least

no need to tell us that the sites are in the Sahel.

squares linear regression. The sites are a) Agoufou (ML-AgG), b) Dahra (SN-Dah), c) Demokeya (SD-Dem), d) Kelma (ML-Kem), e) Wankama Fallow (NE-WaF) and f) Wankama Millet (NE-WaM).